AD-A174 236 THE NEAR-FIELD EFFECTS OF APODISATION ON COHERENT 1/1
ABERRATED OPTICAL SYSTEMS(U) AIR FORCE INST OF TECH
WRIGHT-PATTERSON AFB OH SCHOOL OF ENGI D B ALLRED
UNCLASSIFIED MAR 86 AFIT/GNE/ENP/86M-1 F/G 20/6 NL

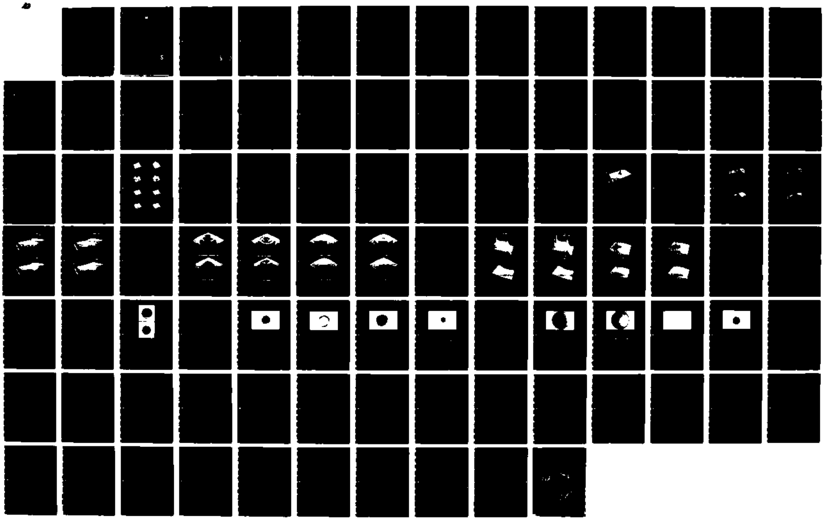

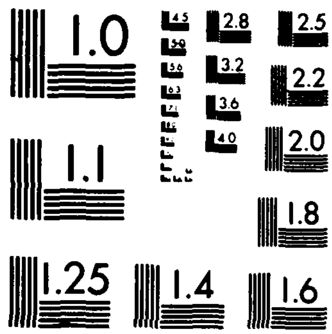

MICROCOPY RESOLUTION TEST CHART
NATIONAL BUREAU OF STANDARDS-1963-A

THE NEAR-FIELD EFFECTS OF APODISATION

ON COHERENT ABERRATED OPTICAL SYSTEMS

THESIS

Daniel B. Allred
Captain, USAF

AFIT/GNE/ENP/86M-1

DEPARTMENT OF THE AIR FORCE
AIR UNIVERSITY
AIR FORCE INSTITUTE OF TECHNOLOGY

Wright-Patterson Air Force Base, Ohio

AFIT/GNE/ENP/86M-1

(1)

THE NEAR-FIELD EFFECTS OF APODISATION

ON COHERENT ABERRATED OPTICAL SYSTEMS

THESIS

Daniel B. Allred
Captain, USAF

AFIT/GNE/ENP/86M-1

Approved for public release; distribution unlimited

AFIT/GNE/ENP/86M-1

THE NEAR-FIELD EFFECTS OF APODISATION ON COHERENT ABERRATED OPTICAL SYSTEMS

THESIS

Presented to the Faculty of the School of Engineering
of the Air Force Institute of Technology
Air University
In Partial Fulfillment of the
Requirements for the Degree of
Master of Science in Nuclear Science

Daniel B. Allred, B.S.
Captain, USAF

March 1986

Preface

The ability to control the ringing effects of Fresnel diffraction is a necessity in high power laser systems. Apodisation is a technique employed in this study to combat this phenomenon.

Apodisation is a topic of current interest in the optics community and certainly to the Air Force with the applications possibility being employed to weapon systems.

I wish to thank Major James P. Mills for proposing the topic and giving such helpful advice and direction; also, Mrs. Pat Mills for her support in the production of the many computer plots. Additionally, I would like to thank Mrs. Phyllis Reynolds who did such an excellent job in typing this thesis; as well as Mr. Ron Gabriel for his outstanding support in the laboratory. Above all, I would like to thank my family; my children Tom and Erica, and my wife Terese for their love, patience, and understanding.

— Daniel B. Allred

<u>Table of Contents</u>

	Page
Preface	ii
List of Figures	v
List of Tables	vii
Abstract	viii
I. Introduction	1
Background	4
II. Theory	7
Near-field Fourier Optics	7
Cylindrical Coordinate Representation	11
On-axis Solutions	12
The Aperture Function	13
Incident Wave (U_{in})	13
Transmittance Function (T)	13
Apodisation (G)	14
Aberrations (A)	15
Lens Term (L)	18
III. Computer Modeling	21
Programs	21
Fourier Transform Method	21
Cylindrical Coordinate Numerical Integration	22
Double Integration Method	23
Computer Predictions	24
Studied Regions	24
The Focal Region	26
The Fresnel Region	33

		Page
IV.	Experimental Results	43
	Measurements of Aberration	43
	The First On-axis Minimum	48
	The Fresnel Region	53
V.	Conclusions	58
	Areas for Further Study	59
Appendix: Computer Codes		60
Bibliography		76
Vita		79

List of Figures

Figure		Page
1.	The Effects of Aberration and Apodisation on Irradiance at the First On-axis Minimum	3
2.	Kirchoff Diffraction Integral Geometry	8
3.	Apodisation Transmittance Function and 3-D Representation	16
4.	Zernike Polynomial Representations of Aberrations	19
5.	Near-field Geometry and Regions of Study	25
6.	Meridional Plane Irradiance Near the Focus a) Topographical (b) Contour Plot from Linfoot and Wolf (17:826)	27
7.	Meridional Plane Modulus Near the Focus	29
8.	Meridional Plane Phase in Radians Near the Focus	29
9.	Cross-sectional Irradiance at the First On-axis Minimum	34
10.	Cross-sectional Phase in Radians at the First On-axis Minimum	36
11.	Meridional Plane Irradiance in the Fresnel Region	39
12.	Meridional Plane Phase in Radians in the Fresnel Region	41
13.	Experimental Arrangement	45
14.	Measurement of Aberration: a) Open Aperture Interferogram, b) Truncated Aperture Interferogram, Aberration (ρ^4) vs ρ	47
15a.	Photograph and Calculated Irradiance for the First On-axis Minimum. Case I: Unaberrated, Unapodised	49

Figure | Page

15b. Photograph and Calculated Irradiance for the First On-axis Minimum, Case II: Aberrated, Unapodised 50

15c. Photograph and Calculated Irradiance for the First On-axis Minimum, Case III: Unaberrated, Apodised 51

15d. Photograph and Calculated Irradiance for the First On-axis Minimum, Case IV: Aberrated, Apodised 52

16a. Photograph and Calculated Irradiance for the Twelfth On-axis Minimum, Case I: Unaberrated, Unapodised 54

16b. Photograph and Calculated Irradiance for the Twelfth On-axis Minimum, Case II: Aberrated, Unapodised 55

16c. Photograph and Calculated Irradiance for the Twelfth On-axis Minimum, Case III: Unaberrated, Apodised 56

16d. Photograph and Calculated Irradiance for the Twelfth On-axis Minimum, Case IV: Aberrated, Apodised 57

List of Tables

Table		Page
I.	Zernike Polynomials and Monomials	18
II.	Experimental Equipment	44

Abstract

The effects of Gaussian apodisation with -0.8 waves of spherical aberration on a coherent optical system was examined. The area of study was in the near-field concentrating on the areas near the focus in the Fresnel region of an f/12 system using optical wavelengths. Computer predictions were made for four cases: unapodised-unaberrated, apodised-unaberrated, unapodised-aberrated, and apodised-aberrated. Predictions were made for cross-sectional planes perpendicular to the optical axis using Fourier optics. Meridional plane predictions were produced using a numerical integration method of determining the Kirchoff integral. Additionally, experimental data are given to compare with the predictions. It is shown that the experimental data matches the computer predictions and that apodisation is an effective method for controlling the ringing due to edge effects and spherical aberrations. Additionally, fine structure corresponding to Young's double slit interference is observed in unapodised cases.

THE NEAR-FIELD EFFECTS OF APODISATION
ON COHERENT ABERRATED OPTICAL SYSTEMS

I. Introduction

This thesis examines the effects of apodisation in the near-field of a coherent optical system with aberrations both experimentally and theoretically. Apodisation is the intentional alteration of the amplitude transmittance of an optical system. It is known that apodisation will effectively smooth the near-field irradiance fluctuations caused by diffraction from the edges of apertures in unaberrated optical systems. *Thompson and Krisl* (25:109) provide graphic evidence of this. This thesis will study the near-field effects of apodisation on aberrated optical systems.

The method undertaken involves theoretical predictions of the apodised response to an aberrated system using scalar diffraction theory. This is done by computer simulations which model the near-field irradiance and phase under four circumstances:

1) the unaberrated and unapodised near-field,
2) the aberrated near-field,
3) the apodised near-field, and
4) the aberrated near-field under apodisation.

In this manner the effects of aberrations and apodisation may be clearly seen.

These predictions are then compared with experimental evidence of the near-field under the same circumstances for spherical aberration.

With the advent of high power lasers, diffraction effects can cause serious damage to components in the optical chain. Control of these effects is necessary for efficient and safe operation of high-power optical systems. This study takes the elementary case of primary aberrations on a plane wave incident upon a lens and aperture. The resulting diffraction effects on the converging wavefront are then analyzed in the Fresnel region with and without aberrations, both under the effects of apodisation and without apodisation.

Figure 1 shows the effects of apodisation on an unaberrated wave, and a wave with third order spherical aberration of -0.8 waves. Figure 1 shows a cross-sectional graph at the first on-axis minimum in irradiance from the focus toward the aperture in an f/12 system with a Fresnel number of 439.021 and a 632.8 nm wavelength. These parameter values are used throughout the study and arise from the experimental system described in Section IV. The irradiance is normalized to one at the focus for the unaberrated unapodised system. The radial coordinate is also normalized (see Section III).

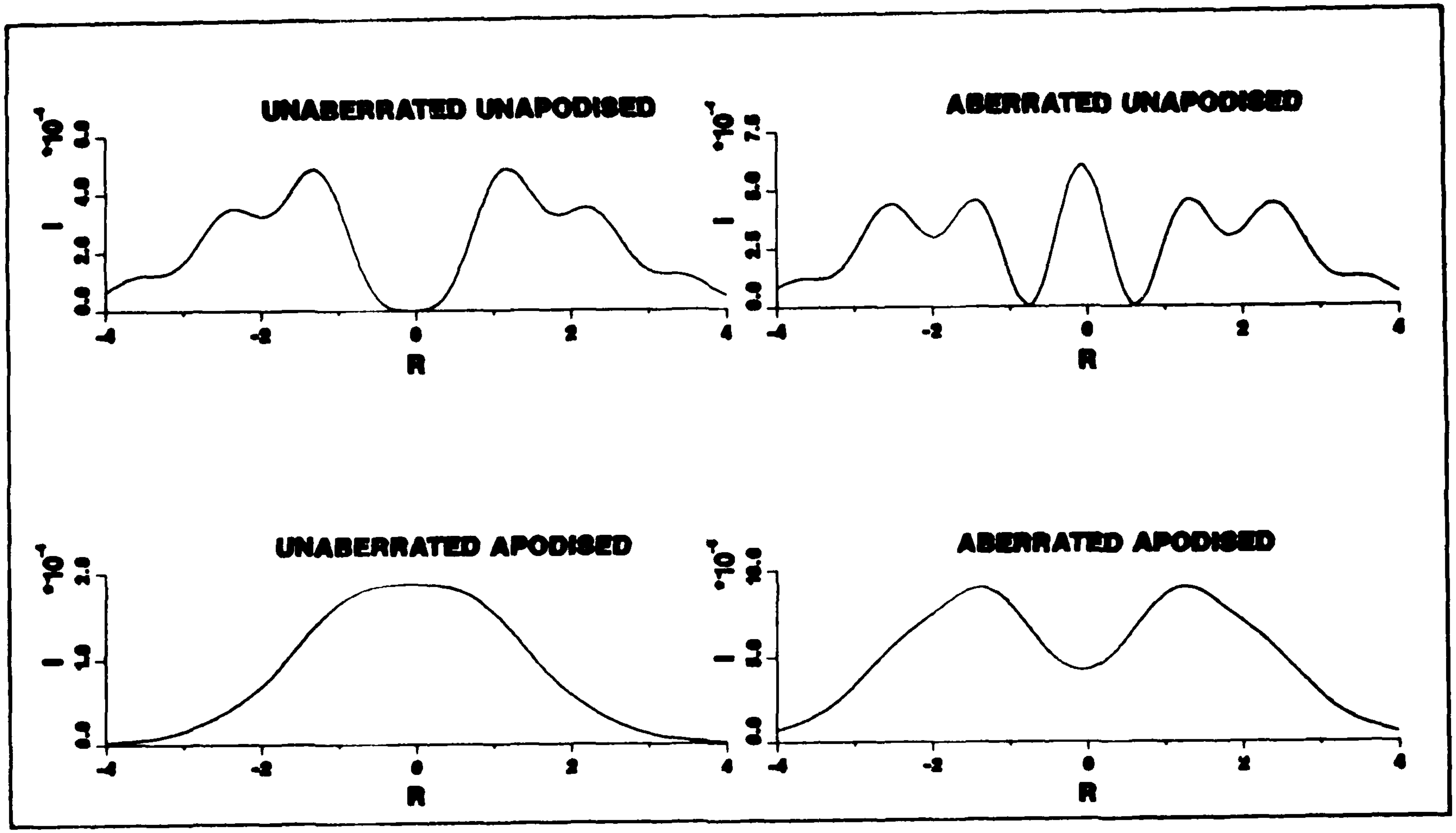

Fig. 1. The Effects of Aberration and Apodisation on Irradiance at the First On-axis Minimum

Background

The near-field has been examined by several authors, most notably are Campbell and DeShazer (4) who evaluated the near-field amplitudes and irradiances using the cylindrical coordinate representation of the Fresnel approximation to the Kirchoff diffraction integral. This was done for Gaussian apodisation. Olaofe (22) has produced an analytical solution to the same integral. Neither of these works consider aberrations.

Harvey and Shack (12) have studied aberrations through the evaluation of the Rayleigh-Sommerfield diffraction formula generalizing into a two-dimensional Fourier transform. This method yields results which do not suffer from the paraxial and Fresnel approximations. This work, however, is mostly concerned with the area of the focal plane.

Avizonis, et al. (1) studied the near-field aberrations with the purpose of gaining insight into their effects at the focus. The evaluation method used was also by the cylindrical Fresnel-Kirchoff integral.

The study of phase has been done principally by Farnell (7; 8; 9) who did his research using microwaves and the calculation methods of Linfoot and Wolf (17) for theoretical evaluation. This was done for both unaberrated and aberrated cases.

Bachynski and Bekefi (2) examined both irradiance and phase on microwave systems and performed a detailed analysis on the effects of aberrations. Most of their work considered the areas at or near the focus. Their work is also quite notable in their prediction and measurement of an axial irradiance in the near-field greater than that at the focus for microwaves.

Work specifically on apodisation has been done by Thompson and Krisl (25) and Kuzimina, et al. (15). Both papers evaluated apodisation effects of various types of apodisers. The latter paper is concerned much more with the focal plane. The former paper demonstrates the ringing decrease in image formation and also in the Fresnel region.

Holmes, et al. (13) examine Gaussian focused beams using numerical integration in cylindrical coordinates of the approximated Kirchoff equation.

The study of apodisation on near-field aberrations is a significant void in the literature, with some work on near-field aberrations and some on apodisation, but none on both. The most complete study of apodisation on aberrations in the image plane is by Mills (21). This thesis is actually an extension to the work done by Mills, in that the apodisation effects on aberrations are now being taken into the near-field. Additionally, this thesis is primarily concerned with spherical aberration, both theoretically and experimentally. Also, this study considers a

very large aperture with respect to the wavelength of light. The aperture diameter is over 21,000 wavelengths wide.

II. Theory

Near-field Fourier Optics

The field amplitude in the near-field is given by solutions to the Helmholtz equation. Scalar diffraction theory is based on the Green's function solution to this equation.

An integral solution to the amplitude $U(x_1,y_1,z)$ in the near-field of an aperture illuminated by a plane wave is given by the Kirchoff diffraction integral:

$$U(x_1,y_1,z) = \frac{-i}{2\lambda}\iint_{\Sigma} U(x_0,y_0)\ \frac{e^{iks}}{s}\ (1 + \cos\chi)\ d\sigma \qquad (1)$$

where λ is the wavelength, k is the wave number $2\pi/\lambda$ and, $U(x_0,y_0)$ is the complex field amplitude in the aperture. The integration is over the wave front in the aperture area Σ using the geometry in Figure 2. The parameter s in Equation (1) is the line segment connecting an arbitrary aperture point Q to an observation point P. The angle χ is between s and the normal to the incident wave front $\hat{n}$. For an unaberrated system the incident wave is a plane wave so $\hat{n}$ is perpendicular to the x_0 and y_0 axes and parallel to z.

Several approximations are now made to simplify Equation (1). The first is the paraxial approximation

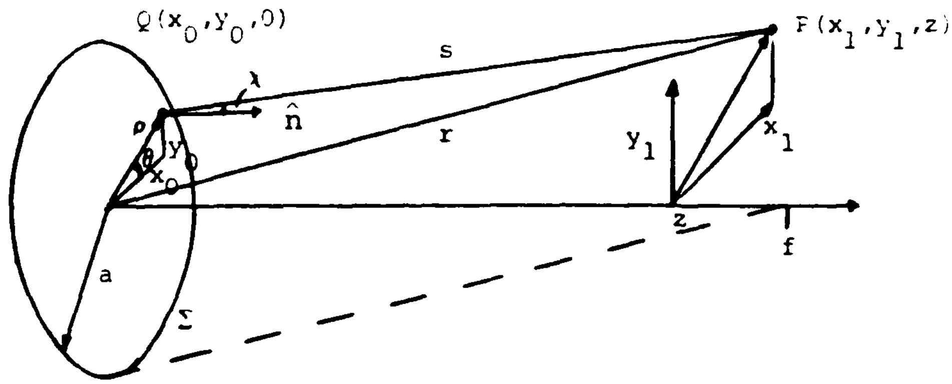

Fig. 2. Kirchoff Diffraction Integral Geometry

and assumes that the angle χ is small so

$$1 + \cos \chi = 2 \tag{2}$$

Secondly, s is approximated to be nearly equal to z. Therefore, s is replaced by z in the denominator of Equation (1). This will not suffice in the argument of the exponent because the error in the approximation would be greatly magnified since it is multiplied by k, a very large number. The Fresnel approximation is therefore applied to s in the exponent. The exact value of s is given by

$$s = z\left[1 + \left(\frac{x_1 - x_0}{z}\right)^2 + \left(\frac{y_1 - y_0}{z}\right)^2\right]^{\frac{1}{2}} \tag{3}$$

Using the binomial expansion on the square root; keeping the first two terms, and then substituting back into the Kirchoff integral gives

$$U(x_1,y_1,z) = \frac{e^{ikz}}{i\lambda z}\iint_{-\infty}^{\infty} U(x_0,y_0)\ \exp\left\{\frac{i\pi}{z\lambda}\left[(x_0-x_1)^2 + (y_0-y_1)^2\right]\right\} dx_0\, dy_0 \tag{4}$$

The limitations due to the approximations are the most severe in the region closest to the lens. The paraxial approximation has an accuracy good to within 5 percent for an angle χ up to 18°. The Fresnel approximation is accurate to the limits of the paraxial approximation. The approximations limit the closest approach to the aperture to

12.7 percent of the focal length. This is as measured on the optical axis from the aperture for an f/12 system.

Equation (4) is recognized as a convolution integral and is quite useful in many applications of diffraction theory. For this thesis it is most useful in a form found after rearranging the exponentials:

$$U(x_1,y_1,z) = \frac{\exp\left(\frac{i2\pi z}{\lambda}\right)}{i\lambda z}\exp\left[\frac{i\pi}{\lambda z}(x_1^2 + y_1^2)\right]\iint_{-\infty}^{\infty}\Big\{U(x_0,y_0)$$

$$\times \exp\left[\frac{i2\pi}{\lambda z}\ (x_0^2 + y_0^2)\right]\exp\left[\frac{-i2\pi}{\lambda z}\ (x_0x_1 + y_0y_1)\right]\Big\}dx_0\, dy_0 \quad (5)$$

where $U(x_0,y_0)$ defines the complex field amplitude in the aperture and is given by

$$U(x_0,y_0) = U_{in}(x_0,y_0)T(x_0,y_0)G(x_0,y_0)A(x_0,y_0)L(x_0,y_0) \quad (6)$$

where U_{in} is the incident amplitude, T is the aperture transmittance, G models the apodisation, A represents the aberrations occurring in the aperture, and L is the disturbance imparted on the field due to a lens. Each of these terms will be looked into in detail later.

Equation (5) is a two-dimensional Fourier transform of the product of the aperture function $U(x_0,y_0)$ and the quadratic exponential term which describes the near-field region dependence of the integrand. This latter term will be called the Fresnel term. Another form for Equation (6) is

$$U(x_1,y_1,z) = \frac{1}{i\lambda z} \exp\left(\frac{i2\pi z}{\lambda}\right)\exp\left[\frac{i\pi}{\lambda z} (x_1^2 + y_1^2)\right]$$

$$\times F\left\{U(x_0,y_0) \exp\left[\frac{i\pi}{\lambda z} (x_0^2 + y_0^2)\right]\right\} \tag{7}$$

where F{} indicates the Fourier transform operator. The transform spatial frequencies are $f_x = x_0/\lambda z$ and $f_y = y_0/\lambda z$. The irradiance is given by

$$I(x_1,y_1,z) = U^*(x_1,y_1,z)U(x_1,y_1,z) \tag{8}$$

where the asterisk denotes the complex conjugate. This equates to

$$I(x_1,y_1,z) = \frac{1}{(\lambda z)^2}\left|F\left\{U(x_0,y_0) \exp\left[\frac{i\pi}{\lambda z}(x_0^2 + y_0^2)\right]\right\}\right|^2 \tag{9}$$

The modulus is then simply the square root of the irradiance:

$$M(x_1,y_1,z) = \frac{1}{\lambda z}\left[\left|F\left\{U(x_0,y_0) \exp\left[\frac{i\pi}{\lambda z}(x_0^2 + y_0^2)\right]\right\}\right|^2\right]^{\frac{1}{2}} \tag{10}$$

Cylindrical Coordinate Representation

If the aperture function $U(x_0,y_0)$ is circularly symmetric then the following substitutions apply:

$$\begin{aligned}
\rho &= (x_0^2 + y_0^2)^{\frac{1}{2}} & x_0 &= \rho\cos\theta \\
\theta &= \arctan(y_0/x_0) & y_0 &= \rho\sin\theta \\
r &= (f_x^2 + f_y^2)^{\frac{1}{2}} & f_x &= r\cos\phi \\
\phi &= \arctan(f_y/f_x) & f_y &= r\sin\phi
\end{aligned} \tag{11}$$

Substitutions are made into Equation (5) and the following trigonometric Bessel function identity applied

$$J_0(b) = \frac{1}{2\pi}\int_0^{2\pi} \exp[-ib\cos(\theta - \phi)]\, d\theta \tag{12}$$

where b is any substitution variable. The irradiance, in cylindrical coordinates is then given by

$$I(r,z) = \left(\frac{2\pi}{\lambda z}\right)^2 \left| \int_0^a U(\rho)\ \exp(i\pi\rho^2/\lambda z) J_0(2\pi r\rho/\lambda z)\ \rho d\rho \right|^2 \tag{13}$$

Equation (13) is the primary equation used to calculate the values of the irradiance both on the optical axis and in the radial direction.

<u>On-axis</u> <u>Solutions</u>. On the optical axis, Equation (13) simplifies since r goes to zero and $J_0(0) = 1$. $U(\rho)$ may still be quite complicated so this simplification does not always lend itself to analytical solutions. It has been solved for the case of an unaberrated unapodised wave and can be integrated directly yielding

$$I(0,z) = \left(\frac{f}{z}\right)^2 \left| \frac{\sin(\phi_0/2)}{(\phi_0/2)} \right|^2 \tag{14}$$

where ϕ_0 is the term arising from the combination of the Fresnel term and the term due to a lens of focal length f placed in the aperture:

$$\phi_0 = \frac{A}{\lambda}\left(\frac{1}{z} - \frac{1}{f}\right)\rho^2 \tag{15}$$

where A is the area of the aperture. Olaofe (22:1654) and Mahajan (19:8) have both solved for the case of Gaussian wave fronts.

For the cases of spherical aberration and apodisation with spherical aberration, the integral becomes analytically unmanageable and requires numerical methods for solution.

The Aperture Function

The Huygens-Fresnel principal states that the field amplitude at any point is given by the superposition of an infinite number of spherical waves radiating from an infinite number of points in the aperture. Thus, the aperture function describes the scalar field amplitude in the aperture. This is given by Equation (6):

$$U(x_0,y_0) = U_{in}(x_0,y_0)T(x_0,y_0)G(x_0,y_o)A(x_0,y_0)L(x_0,y_0) \qquad (16)$$

Each term will be examined one at a time.

Incident Wave (U_{in}). This term is simply the complex field amplitude incident upon the aperture. In this study this will always be considered as a plane wave of unit amplitude.

Transmittance Function (T). The transmittance function defines how the boundary conditions of the aperture allow the incident infinite plane wave to transmit through

the aperture. For the case of a circular aperture this is a circle function of unit amplitude out to the aperture boundary:

$$T(\rho) = \mathrm{circ}(\rho/a) = \begin{cases} 1 & 0 \leq \rho \leq a \\ 0 & \text{otherwise} \end{cases} \tag{17}$$

<u>Apodisation (G)</u>. With a Gaussian apodiser the transmittance is a Gaussian function truncated by the edges of the circle function. The apodiser could be a complex function but this study will consider only real Gaussian apodisers for three reasons:

1) the Fourier transform of a Gaussian is itself a Gaussian,
2) the impulse response is real and positive, and
3) there are strong similarities with some laser wave fronts.

The equation for a Gaussian is

$$G(\rho) = \exp(-2\gamma\rho^2) \tag{18}$$

where $\gamma = (a/w)^2$, w being the irradiance e^{-2} beam radius. In this study $\gamma = 3/2$. Often the coefficient 2γ is replaced by $1/\alpha_0^2$ in the literature. In either case the apodisation function considered here has the form

$$G(\rho) = \exp(-3\rho^2) \tag{19}$$

This function has the property of having a transmittance of 0.05 at the aperture boundary thus only weakly truncating

the wave front as in Figure 3. The weak truncation eliminates almost all the edge effects as seen in the work by Mills (21:3).

Aberrations (A). The aberration of primary importance in this study is third order spherical aberration. It is represented mathematically by the Zernike polynomials and monomials which represent the aberrated wave in the aperture. A brief discussion of the Zernike polynomials follows which parallels the treatment by Malacara (20:489-505) and Born and Wolf (3:464-466) which should be consulted for greater detail.

The Zernike polynomials are orthonormal terms which are balanced polynomials that provide the highest Strehl ratio at the paraxial focus. The polynomials satisfy the condition

$$\int_0^1 \int_0^{2\pi} Z_n^{\ell *} Z_m^{\ell} \rho \, d\rho \, d\theta = \frac{\pi}{n+1} \delta_{nm} \tag{20}$$

where δ_{nm} is the Kronecker delta function and the asterisk represents the complex conjugate. The function Z_n^{ℓ} can be broken into a radial term and an axial term or

$$Z_n^{\ell} = R_n^{\ell}(\rho) \exp(i\ell\theta) \tag{21}$$

where n is the degree of the polynomial and ℓ is the angular dependence. The radial distance ρ is normalized to the aperture radius. Both n and ℓ must either be odd or

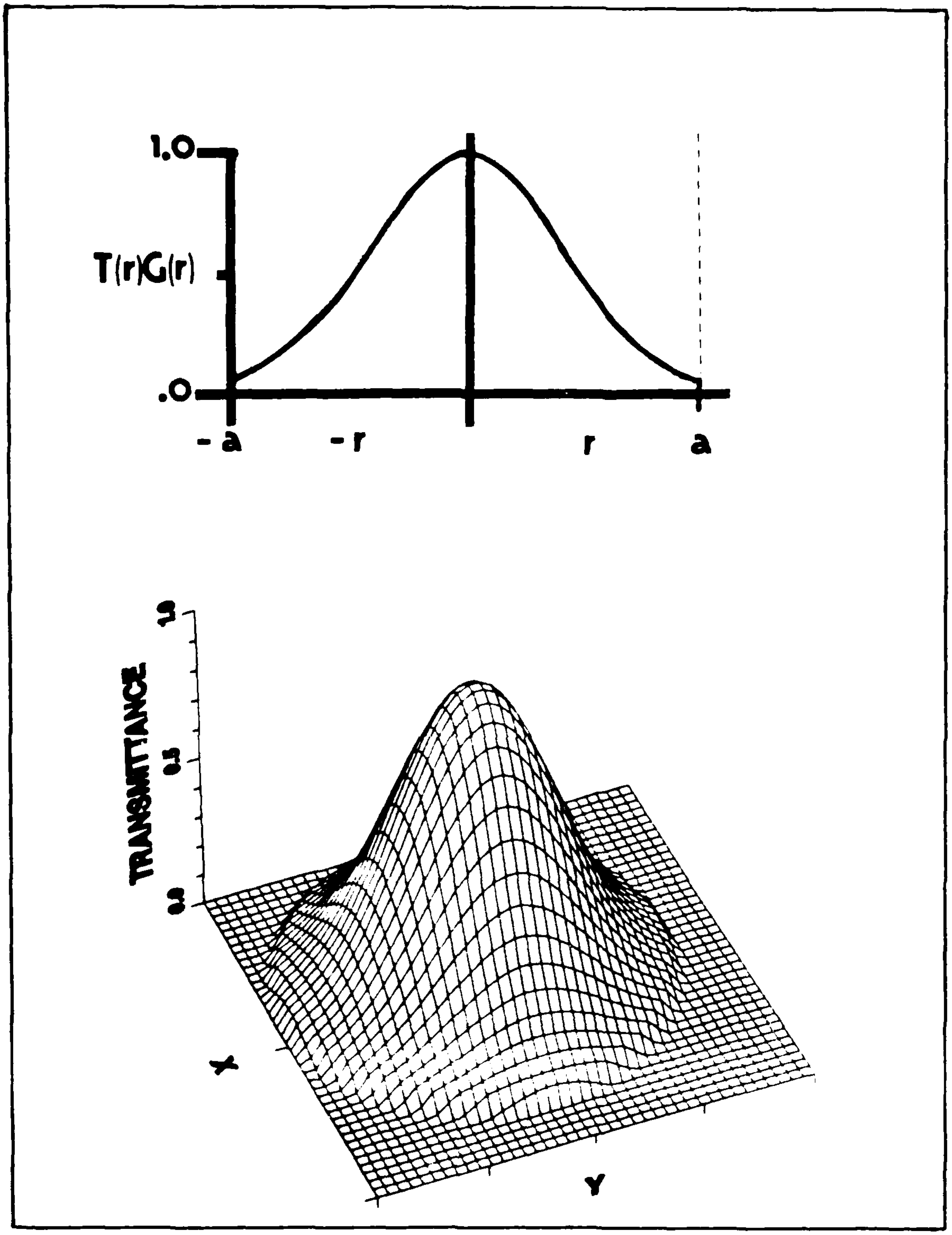

Fig. 3. Apodisation Transmittance Function
and 3-D Representation

even. A radial polynomial R_n^ℓ exists for each pair of numbers n and $|\ell|$. Also

$$R_n^{\ell} = R_n^{-\ell} = R_n^{|\ell|} \tag{22}$$

When n is even the polynomial is symmetrical and the exponents of the polynomial terms are even. When n is odd the polynomial is antisymmetric and the exponents are odd. The radial polynomials are found by the relation

$$R_n^{n-2m}(\rho) = \sum_{s=0}^{m} (-1)^s \left[\frac{(n-s)!}{s!\,(m-s)!\,(n-m-s)!} \rho^{n-2s} \right] \tag{23}$$

For defocus, $n = 2$ and $\ell = 0$. For third order spherical aberration, $n = 4$ and $\ell = 2$. Since n is even in both cases there is no angular dependence.

The Zernike polynomials may be converted to rectangular coordinate monomial forms by the substitutions of $x = \rho\sin\theta$ and $y = \rho\cos\theta$. The Zernike polynomials and monomials are displayed in Table I which is reprinted from Malacara. Only the terms which correspond to primary aberrations have been kept. Coma and spherical aberrations listed are third order.

When the polynomials are included in the aperture function they are in the argument of a complex exponential to represent the phase disturbance on the wavefront. They are also multiplied by the amplitude of the aberration

TABLE I

ZERNIKE POLYNOMIALS AND MONOMIALS (20:493)

n	m	n-2m	Polynomials	Monomials	Meaning
0	0	0	1	1	Constant term
1	0	1	$\rho\sin\theta$	x	Tilt in x
	1	-1	$\rho\cos\theta$	y	Tilt in y
2	0	2	$\rho^2\sin 2\theta$	2xy	Astigma. ±45°
	1	0	$(2\rho^2-1)$	$-1+2y^2+2x^2$	Focus shift
	2	-2	$\rho^2\cos 2\theta$	y^2-x^2	Astigma. 0°,90°
3	1	1	$(3\rho^3-2\rho)\sin\theta$	$-2x+3xy^2+3x^3$	x axis coma
	2	-1	$(3\rho^3-2\rho)\cos\theta$	$-2y+3y^3+3x^2y$	y axis coma
4	2	0	$6\rho^4-6\rho^2+1$	$1-6y^2-6x^2+6y^4$ $+12x^2y^2+6x^4$	Spherical

in wavelengths. Plots of the Zernike polynomials are in Figure 4.

Lens Term (L). The inclusion of a converging lens creates a spherical wavefront with its center at the focus. The phase disturbance for the lens is represented by

$$L(\rho) = \exp(-i\pi\rho^2/\lambda f) \tag{24}$$

Equation (24) is a quadratic approximation to the actual spherical wavefront. This representation for the lens effects is pervasive in the literature and is developed by Goodman (10:80) as well as other sources. A converging

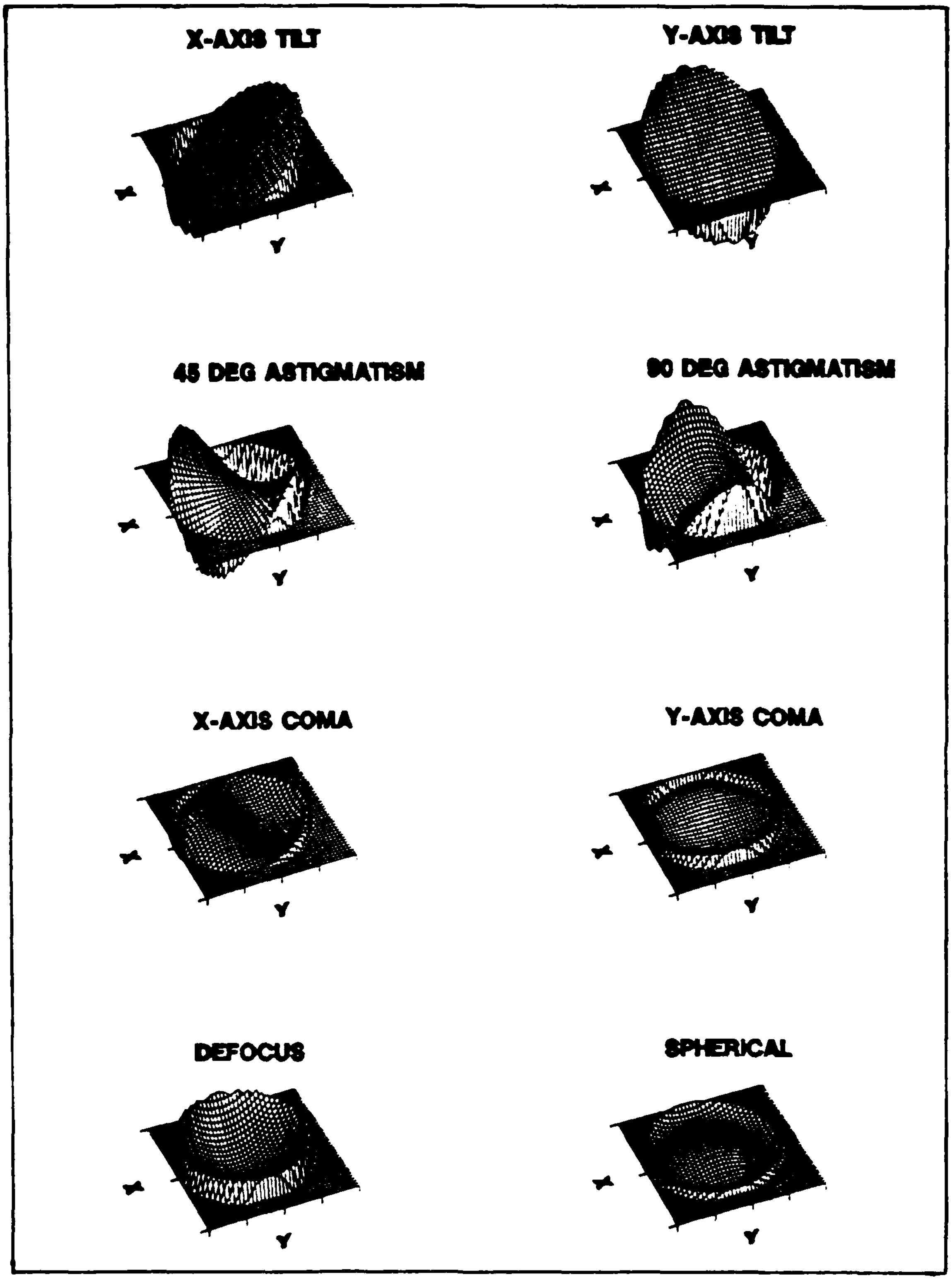

Fig. 4. Zernike Polynomial Representations of Aberrations

lens is always considered to be in the aperture for all cases in this thesis.

III. Computer Modeling

Programs

The prediction of the irradiance, modulus, and phase at various points in the image field of an aperture was done by computer modeling. Three main approaches were used and are described below.

Fourier Transform Method. Values for the irradiance, modulus, and phase can be obtained for cross-sectional planes by performing the two-dimensional Fourier transform of Equations (9) and (10). This code is based on creating a two-dimensional array of the aperture function, multiplying by the Fresnel term, and then taking the Fourier transform. The code was initially developed by Mills (21) to give results in the focal plane. Its modification now allows computation for results in the near-field. The code is named N256.FOR and is included in the appendix. The Fourier transform is calculated by the IMSL (14) routine FFT3D.

To be generic for any system, Equation (9) was normalized by the variable substitutions

$$x_n^0 = x_0/a \qquad y_n^0 = y_0/a$$

$$x_n^1 = x_1/(\lambda z/a) \qquad y_n^1 = y_1/(\lambda z/a)$$

$$I_n = I_0(x_0, y_0, z)/(\pi a/\lambda f)^2 \tag{25}$$

This yields the normalized equation after dropping subscripts

$$I(x_1,y_1,z) = \frac{1}{(\pi c)^2}\left|F\left\{\Sigma\Phi(x_0,y_0)\exp\left[i\pi FN\frac{(1-c)}{c}\right.\right.\right.$$
$$\left.\left.\left.\times\ (x_0^2 + y_0^2)\right]\right\}\right|^2 \qquad (26)$$

where c is simply the ratio z/f and FN is the Fresnel number of the system, $a^2/\lambda f$. In this study a Fresnel number of 439.021 was used which uses the parameters of the experimental system with $\lambda = 6.328 \times 10^{-5}$ cm, an aperture radius of 0.66675 cm, and a focal length of 16.002 cm. The reasons for these values are defined by the experiment. With the paraxial approximation on this system, accuracy to within 5 percent occurs when z/f is less than or equal to 0.12. The areas under study here are well within the approximations used.

Cylindrical Coordinate Numerical Integration. The near-field irradiance can also be given by Equation (13) which uses cylindrical coordinates and the zero order Bessel function of the first kind. As also shown by Mahajan (18:3036), it is normalized with the substitutions

$$\rho_n = \rho/a,\ r_n = r/(\lambda f/2a),\ I_n(r_n) = I_0/(\pi a^2/\lambda f)^2 \qquad (27)$$

Equation (13) now becomes, after dropping subscripts

$$I(r,z) = 4\left(\frac{1}{c}\right)^2\left|\int_0^1\left[\exp\ i\Sigma\Phi(\rho)\right]\ J_0\left(\frac{\pi f r\rho}{z}\right)\rho d\rho\right|^2 \qquad (28)$$

where $\Sigma\Phi(\rho)$ is the sum of the Fresnel and aberration terms.

Radial data can be computed using this equation as well as data on the optical axis. The codes use Simpson's rule integration and the Bessel function is computed by the IMSL routine MMBSJO (14). An alternative to using the IMSL routine is to use the Bessel identity (5:188)

$$J_0(b) = \frac{2}{\pi}\int_0^{\frac{\pi}{2}} \cos(b\sin\phi)\,d\phi \tag{29}$$

using numerical integration in the subroutine to calculate $J_0(b)$. The values in the meridional plane are calculated by this method by the code MERID.FOR which is also included in the appendix.

Double Integration Method. The double integration method follows directly the method used by Bachynski and Bekefi (2:430) in the generation of their data, as well as the works done by Lee and Farnell (16:273)

$$U(r,z) = \frac{-ika^2U_{in}}{2\pi zf}\exp[ik(f-z)]\int_0^1\int_0^{2\pi}\exp(-G\rho^2)$$

$$\times\ \exp[-ip\rho^2 - iq\rho\cos(\theta-\psi) + ikV(\rho,\theta)]\,\rho\,d\rho\,d\theta \tag{30}$$

where

$p = (ka^2/2zf)(f-z)$

$q = (ka/f)r$

V = aberration terms

G = Gaussian apodisation constant

Equation (30) utilizes the cylindrical coordinate system previously mentioned, but does not utilize the Bessel identity in Equation (12) keeping the angular dependence in the integral. This allows the computation of non-circularly symmetric aperture functions which can be used to study the effects of coma, astigmatism, and tilt aberrations. This program utilizes the IMSL integration routine DBLIN (14).

This method provides very accurate results due to the cautious Romberg integration method used by the IMSL routine. A great drawback to this method is the enormous amount of computer time which the code takes. The program which utilizes this method, IRAD.FOR, is also included in the appendix.

Computer Predictions

Studied Regions. There were two main regions of the near-field which were closely studied: the area near the focus and the area near $z/f = 0.95$, as shown in Figure 5. The focal area was studied because there was existing data to check the accuracy of the codes' predictions. Also, it is an area of interest in that it provides a unique opportunity to see the physical responses in the transition from Fresnel to Fraunhofer diffraction. All plots were made with the graphics software package DISSPLA (6).

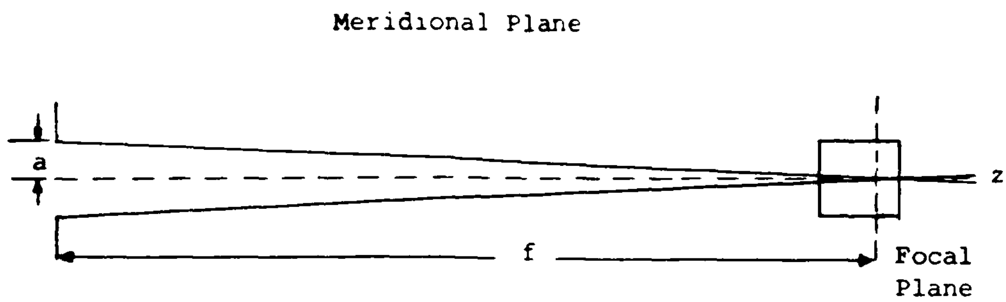

The near-field of an f/12 system. The boxed area is the enlarged area below.

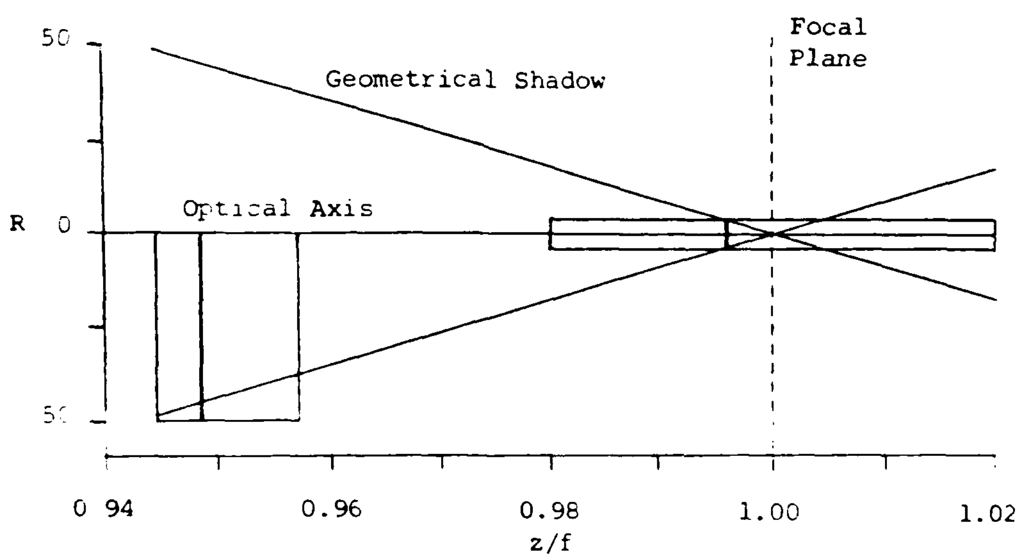

Fig. 5. Near-field Geometry and Regions of Study

The area near $z/f = 0.95$ was studied to observe the effects of aberrations and apodisation in the Fresnel region. Areas closer to the aperture were found to require enormous computer resources far beyond the capabilities of the systems available. The creation of enormous two-dimensional arrays is required to accurately predict the cross-sectional disturbance in these areas. Even at $z/f = 0.95$, cross-sectional arrays were incalculable due to the required size for accurate measurement. A look at the photographs in the next section demonstrates the vast amount of resources required to predict, store, and provide an accurate output of such large amounts of information. Fortunately, radial plots in this region could be produced without too much difficulty. Radial plots are sufficient because the cross-sectional plane is circularly symmetric.

<u>The Focal Region</u>. The focal region under study consists of the area from $z/f = 0.98$ to $z/f = 1.02$ and from $r_n = -4.0$ to 4.0 using the normalized radial coordinates

$$r_n = r(2a/\lambda f) \tag{31}$$

The system studied throretically, used the parameters of the experimental system with a Fresnel number of 439.021.

The meridional plane over the focal region is given in Figure 6. The meridional plane is the plane defined when the angle ϕ is zero as seen in Figure 2. It can be

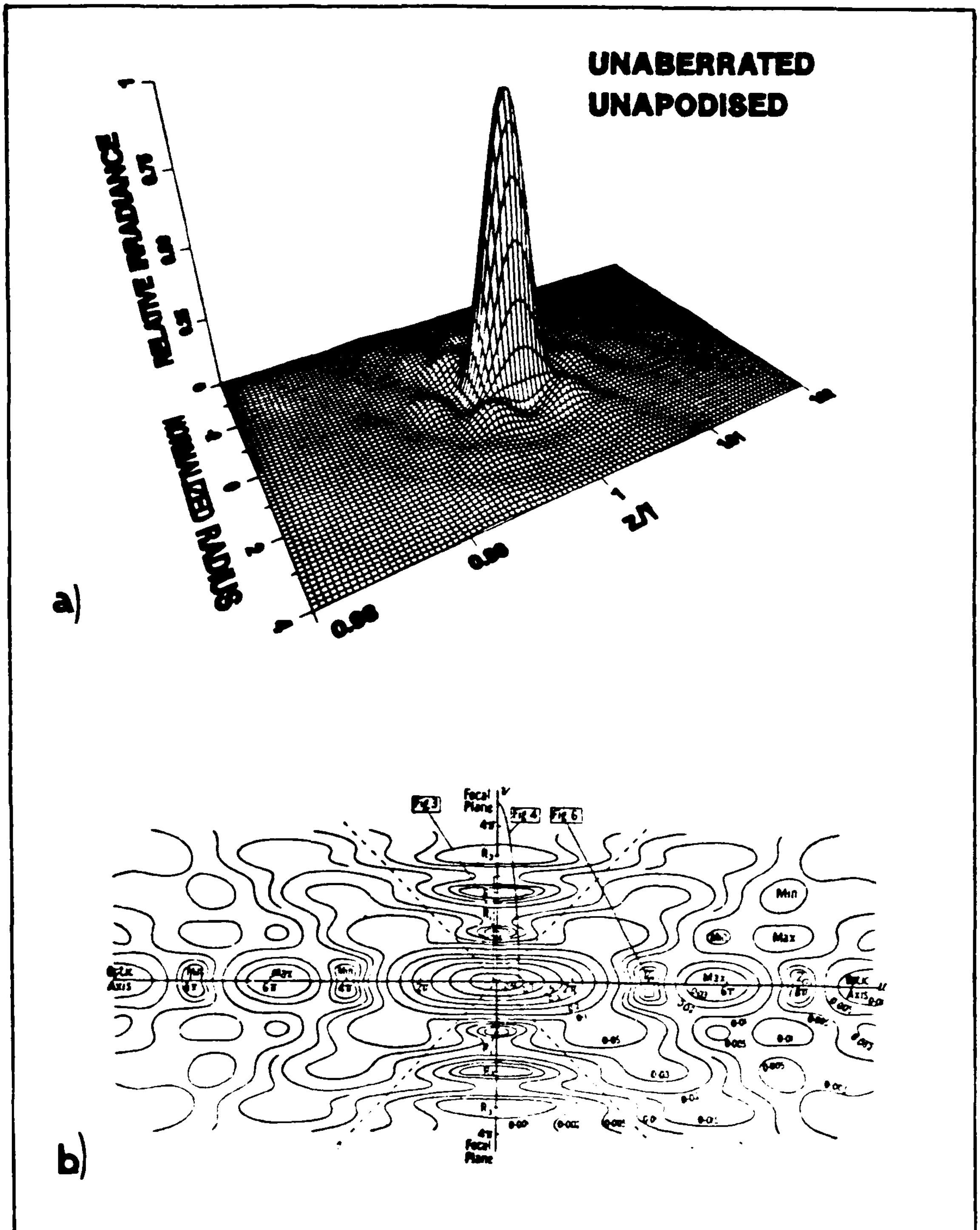

Fig. 6. Meridional Plane Irradiance Near the Focus
a) Topographical; b) Contour Plot from
Linfoot and Wolf (17:826)

easily compared with the two-dimensional contour plot from Linfoot and Wolf (17:826) which has a different coordinate system covering a slightly smaller area along the optical axis, but the same area on either side of the axis. This qualitatively demonstrates the accuracy of the code MERID.FOR which produced the plotted data.

The effects of apodisation and spherical aberration on the entire focal area in the meridional plane can be seen quite dramatically in Figure 7. The spherically aberrated modulus changes the values seen in the unaberrated plot. Phase is plotted in Figure 8. The peak in modulus corresponds to the circle of least confusion. When the apodiser is in place, the ringing in the unaberrated system completely disappears in this region. In the aberrated system, the ringing is very much reduced but not completely eliminated. In all cases of apodisation, there is a significant reduction in amplitude of the peak values. This is due to the attenuation of the energy allowed to pass through the aperture by the absorbing apodiser. Additionally, the edge effects have been dramatically reduced, since the edges are only 5 percent as high as in the unapodised aperture.

Many of the two pi jumps in phase are due to a recycling of the arctangent function used to calculate the phase value. A false impression of a phase jump is thus given. A graphic indication of the rapid phase changes

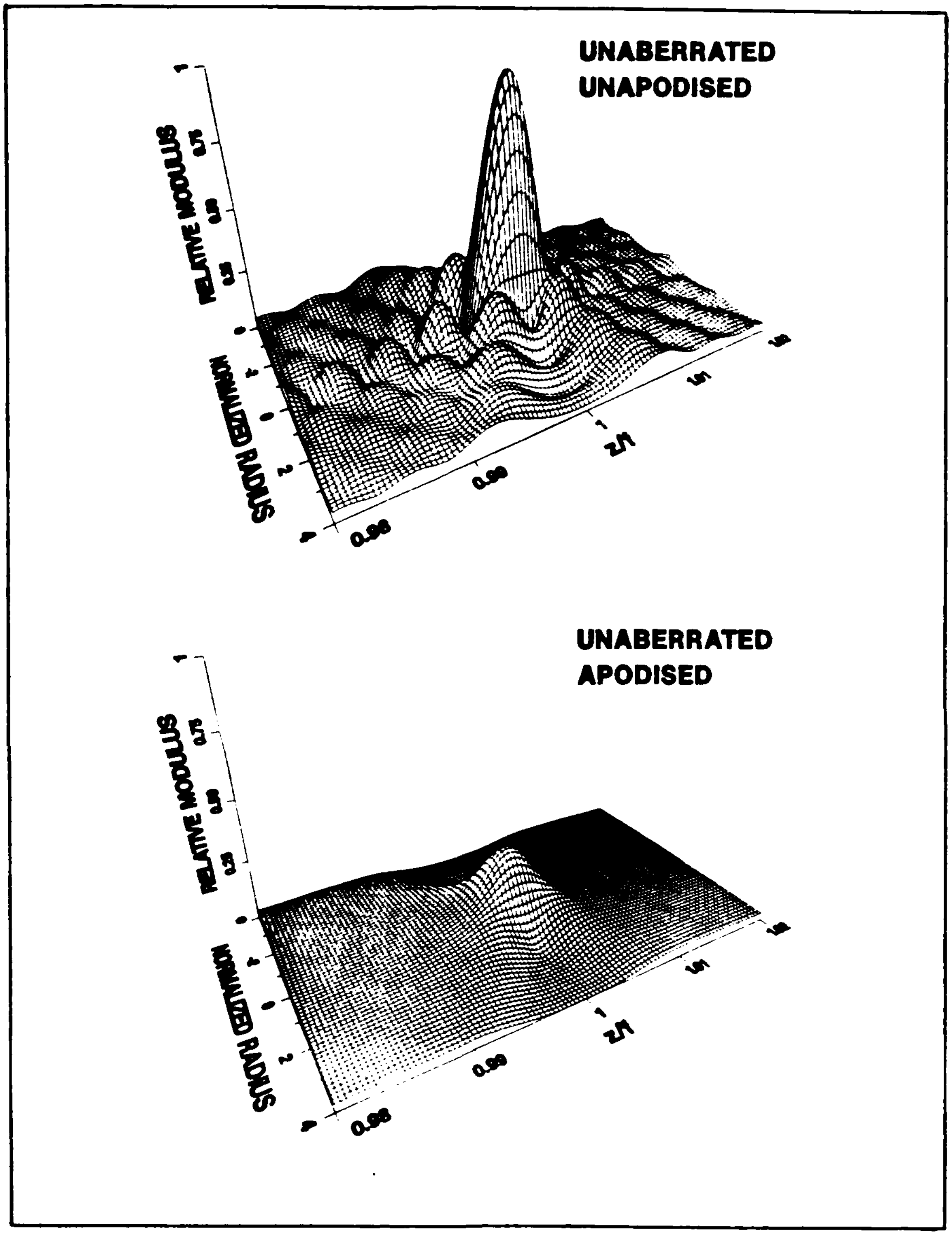

Fig. 7. Meridional Plane Modulus Near the Focus

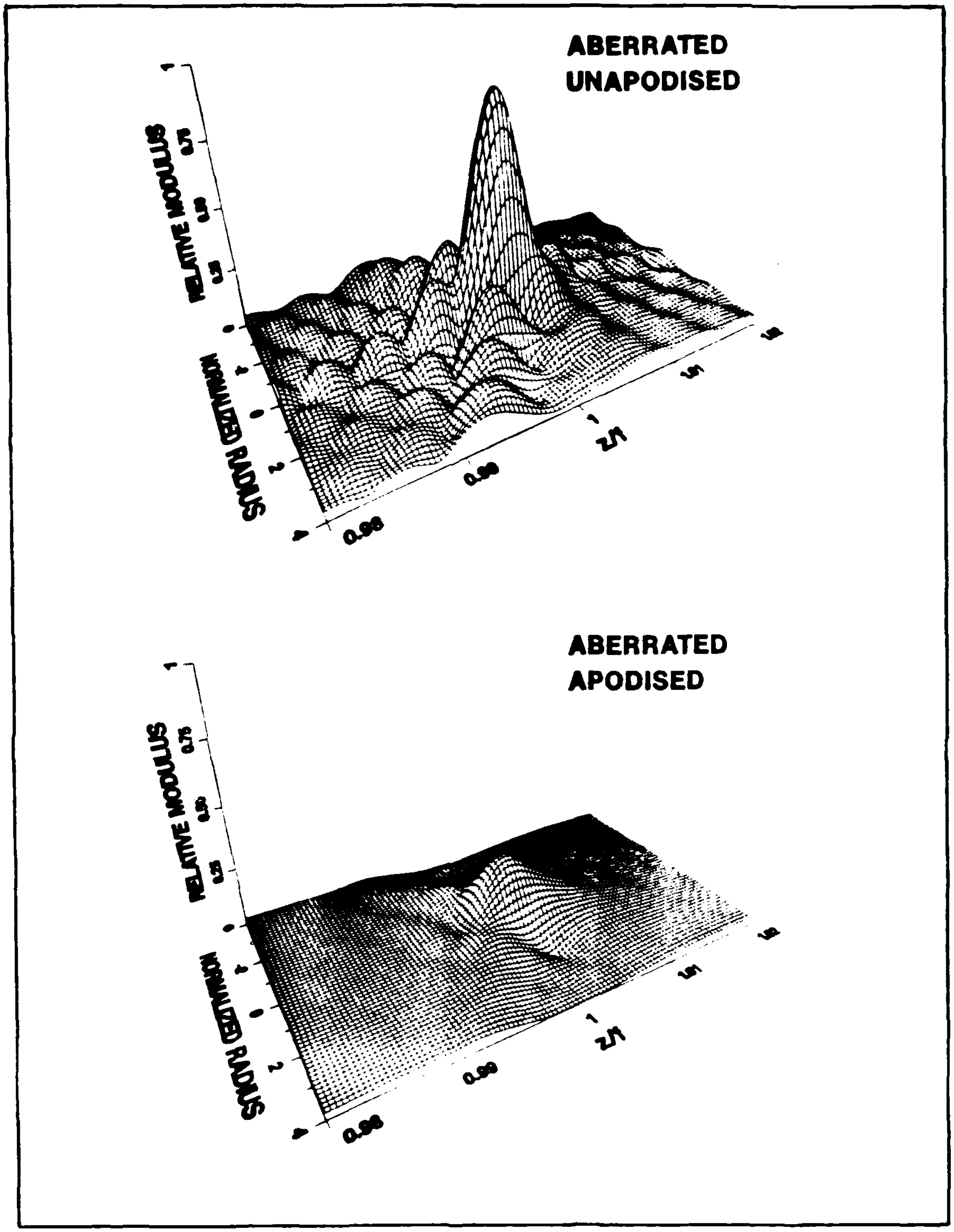

Fig. 7--Continued

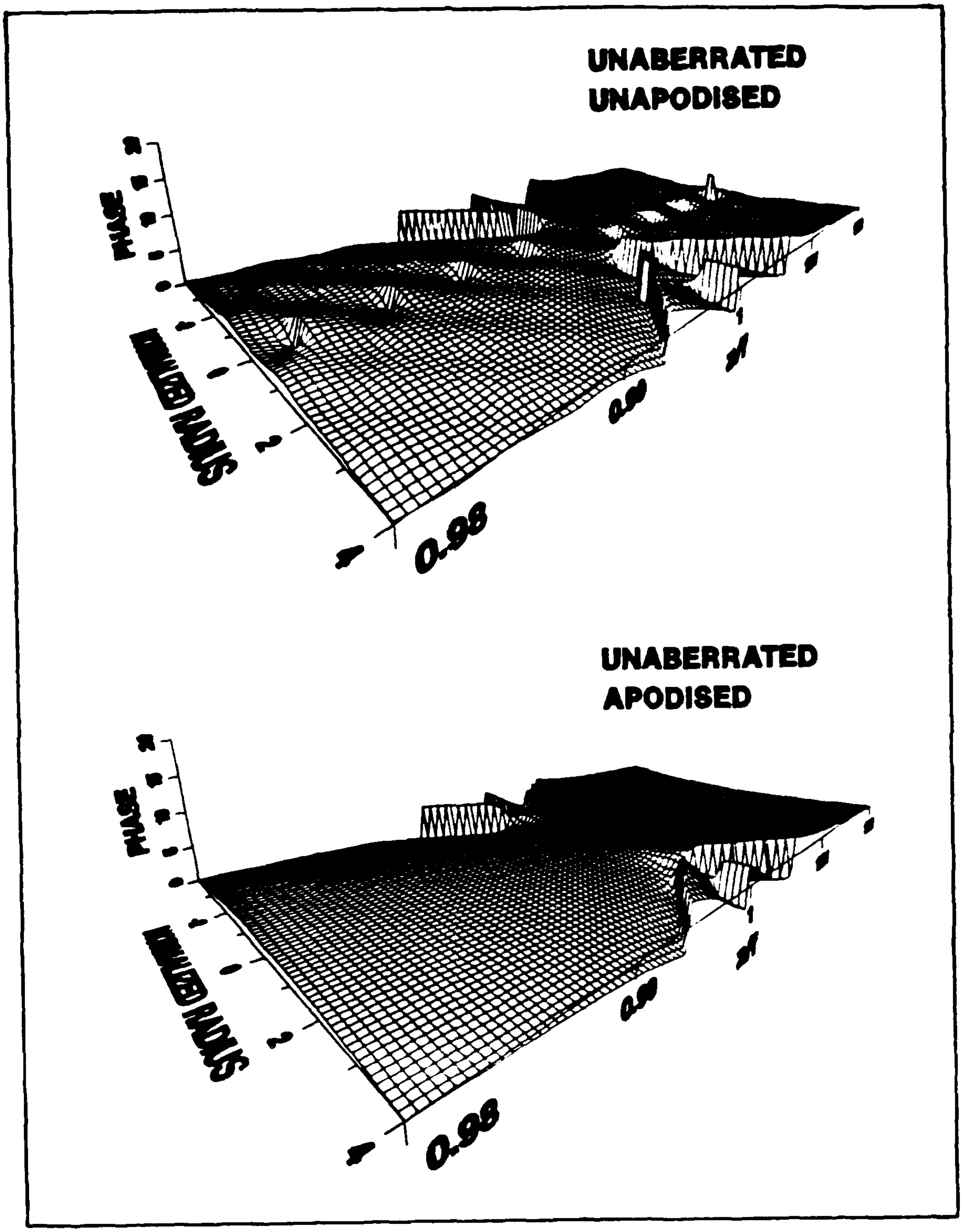

Fig. 8. Meridional Plane Phase in Radians
Near the Focus

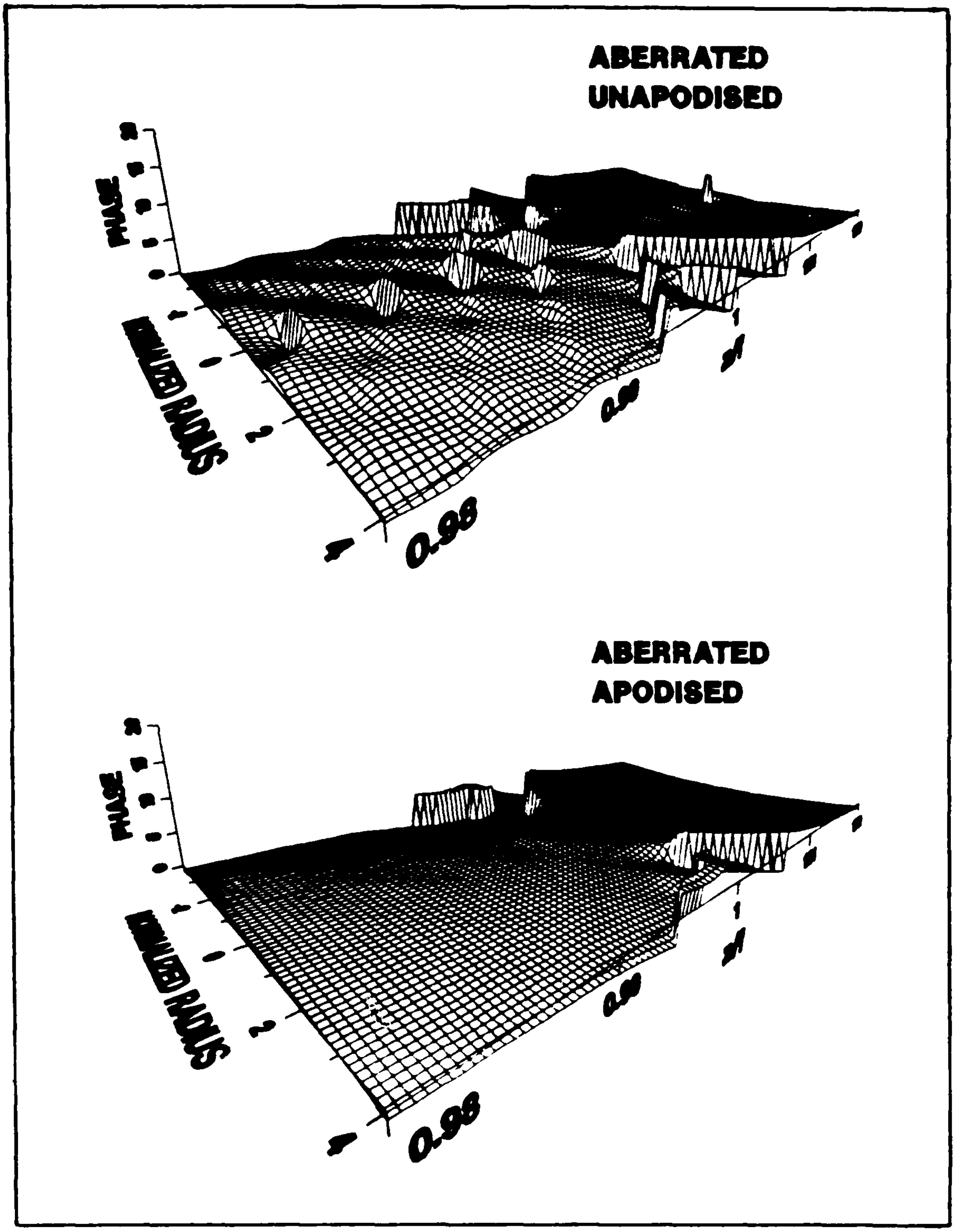

Fig. 8--Continued

occurring in the aberrated plots prior to the focal plane is easily seen however. The phase shifts behind the focal plane are real and can be seen to represent the diverging rings in the modulus plot.

Scalar diffraction theory predicts the existence of on-axis zeros in irradiance in the intervals predicted by Equation (14). This is the first on-axis zero seen in Figure 5 on the aperture side of the focus. The theoretical irradiance cross-sections which include this first on-axis zero appear in Figure 9 for the four cases under study, and phase is shown in Figure 10. The two-dimensional centerline plots were given in Figure 1 in Section I. As can be clearly seen, the on-axis zero disappears when aberrated with -0.8 waves of spherical aberration. Additionally, apodisation removes the on-axis zeros as well as reducing the amplitude of the modulus over the entire structure. The apodisation also reduces the intensified ringing caused by the aberration.

The Fresnel Region. The region centered on z/f = 0.95 was studied using radial plots from the optical axis outward to normalized radial distance of 50.0. The z-axis was taken from the 13th on-axis zero from the focus to the 10th. The values were found by solving Equation (14) for minima. Mahajan (19:8) gives the relation as

$$(z/f)_n = FN/(FN+2n), \quad n = 1, 2, 3, \ldots \qquad (32)$$

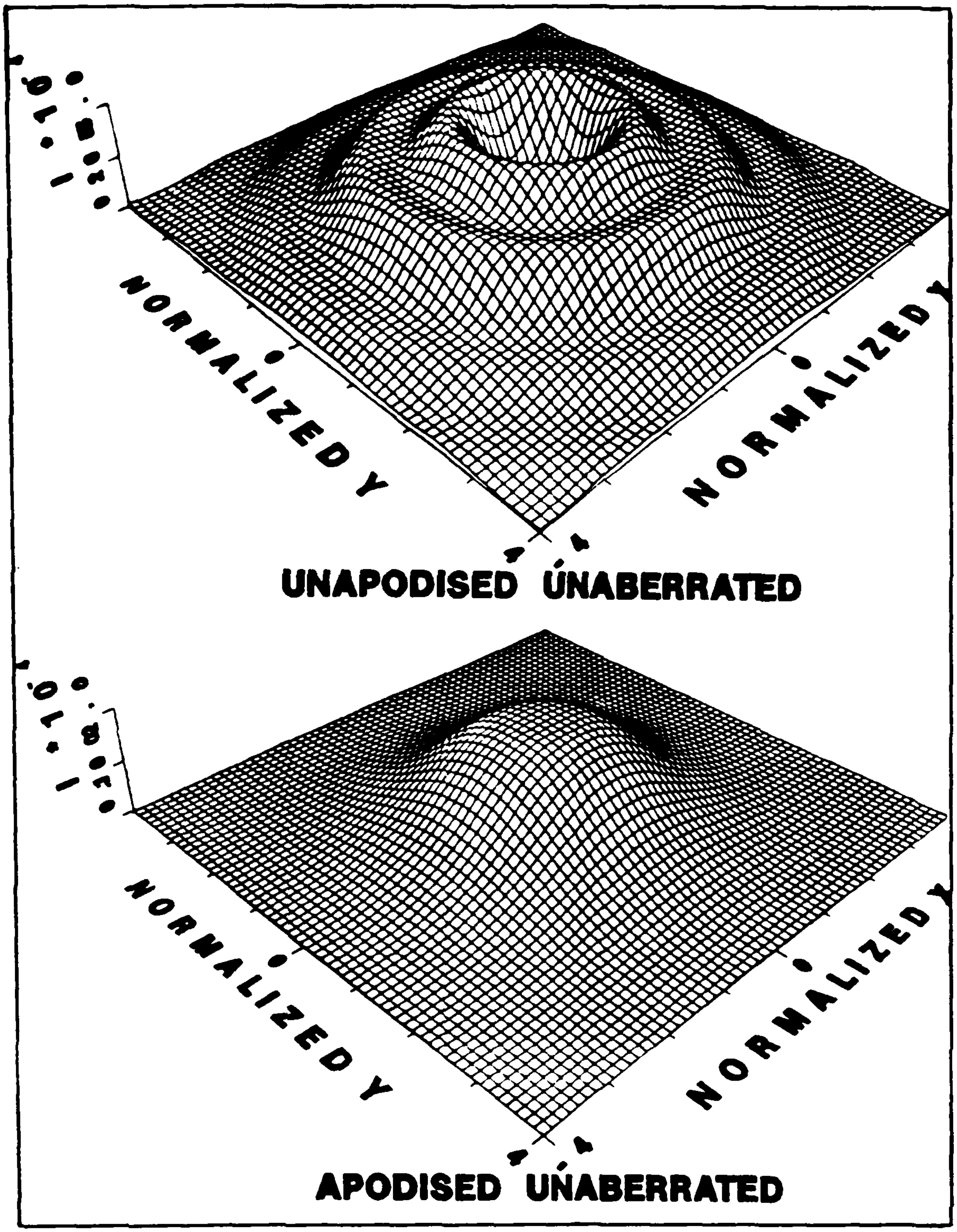

Fig. 9. Cross-sectional Irradiance at the First On-axis Minimum

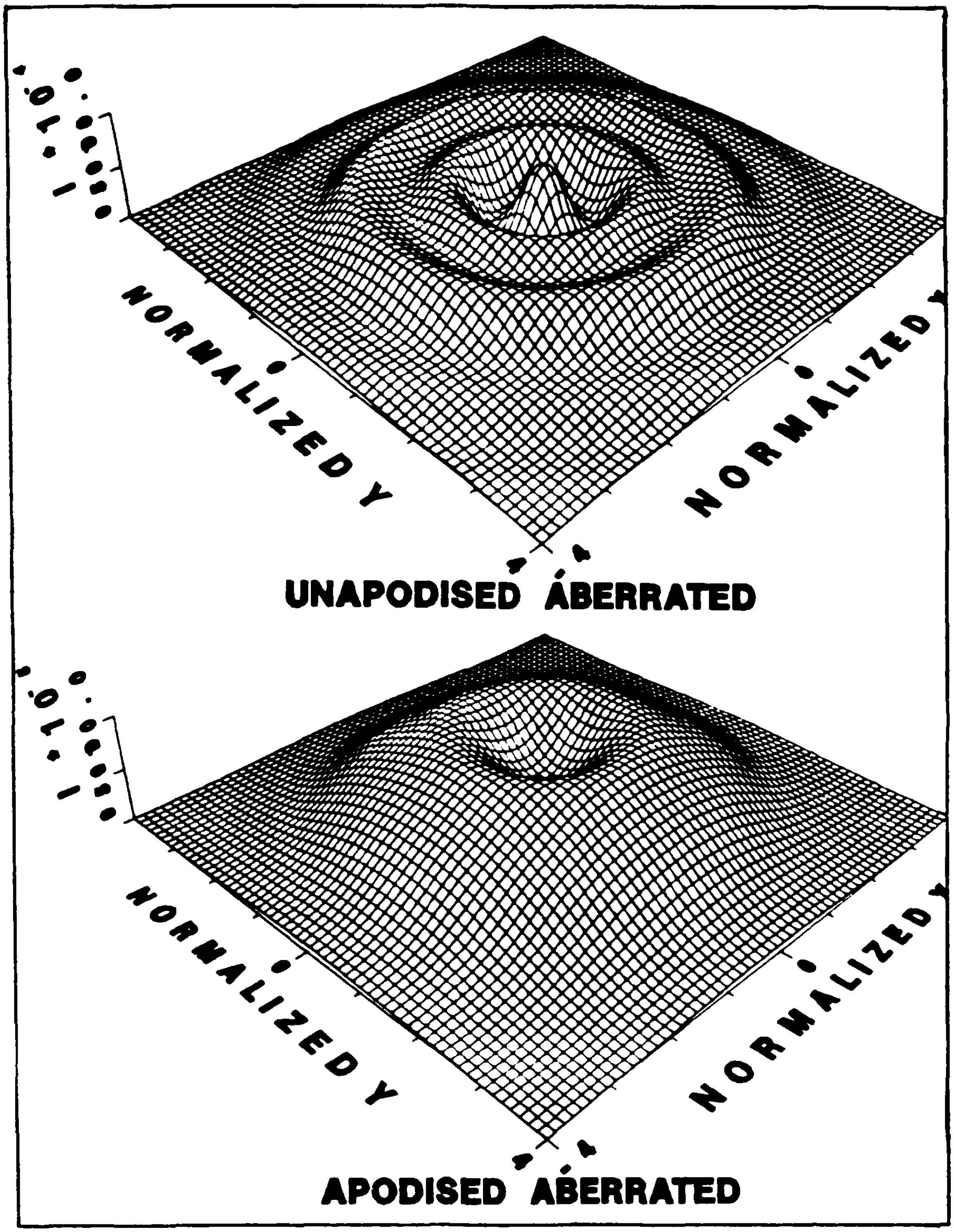

Fig. 9--Continued

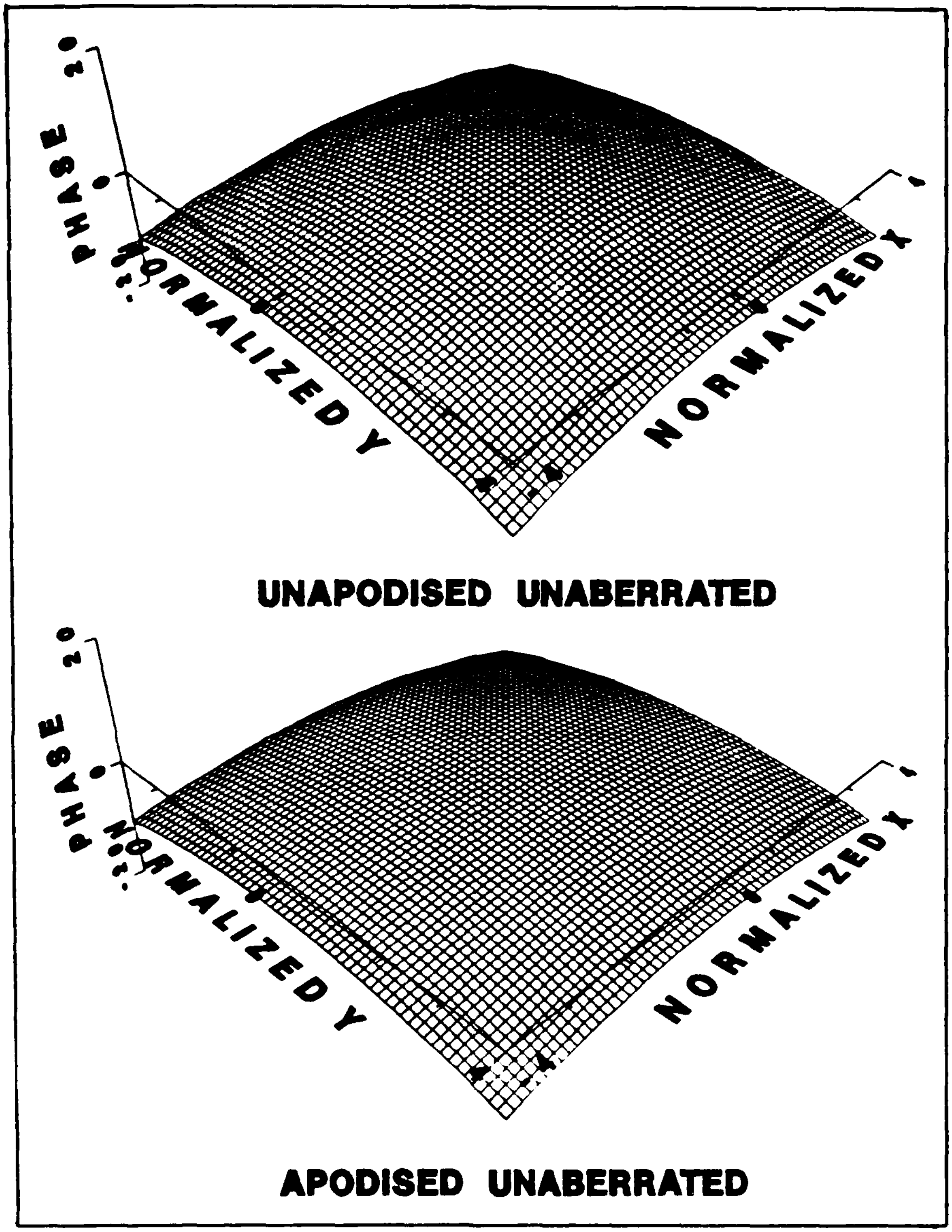

Fig. 10. Cross-sectional Phase in Radians at the First On-axis Minimum

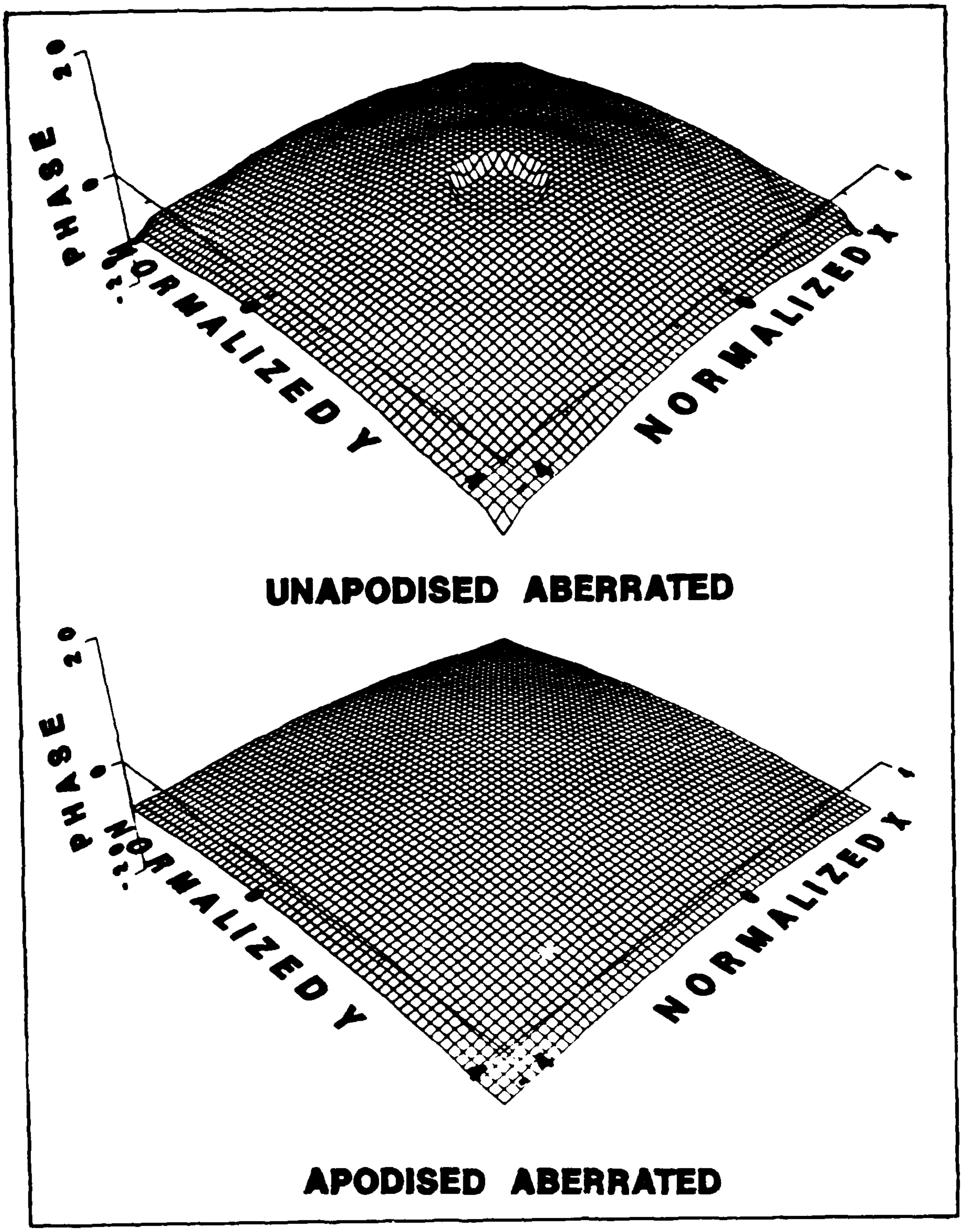

Fig. 10--Continued

where n is the number of the on-axis zero desired. In this case the values of z/f where n = 13 and n = 10 define the boundaries of the region. The irradiance plots of the four considered cases in this region are in Figure 11 and the corresponding phase plots are in Figure 12. There are some significant predictions in these plots. The unapodised unaberrated plot predicts an addition of a fine wave structure riding on the Fresnel pattern. This fine structure seems to intensify as the radius increases. The aberrated plot predicts a more extreme radial pattern with a more intense outer ring. Additionally, the fine structure is slightly reduced in the area outside the outer ring. The fine structure has a period corresponding to that given by Young's double slit interference with the slits taken at the aperture edges. The apodised plot indicates what appears to be a complete loss of ringing. On the aberrated plot, the apodisation again is seen to substantially reduce the ringing.

The first minimum cross-sectional plane and the 12th are studied experimentally in the next section and provide interesting comparisons with the computer predictions.

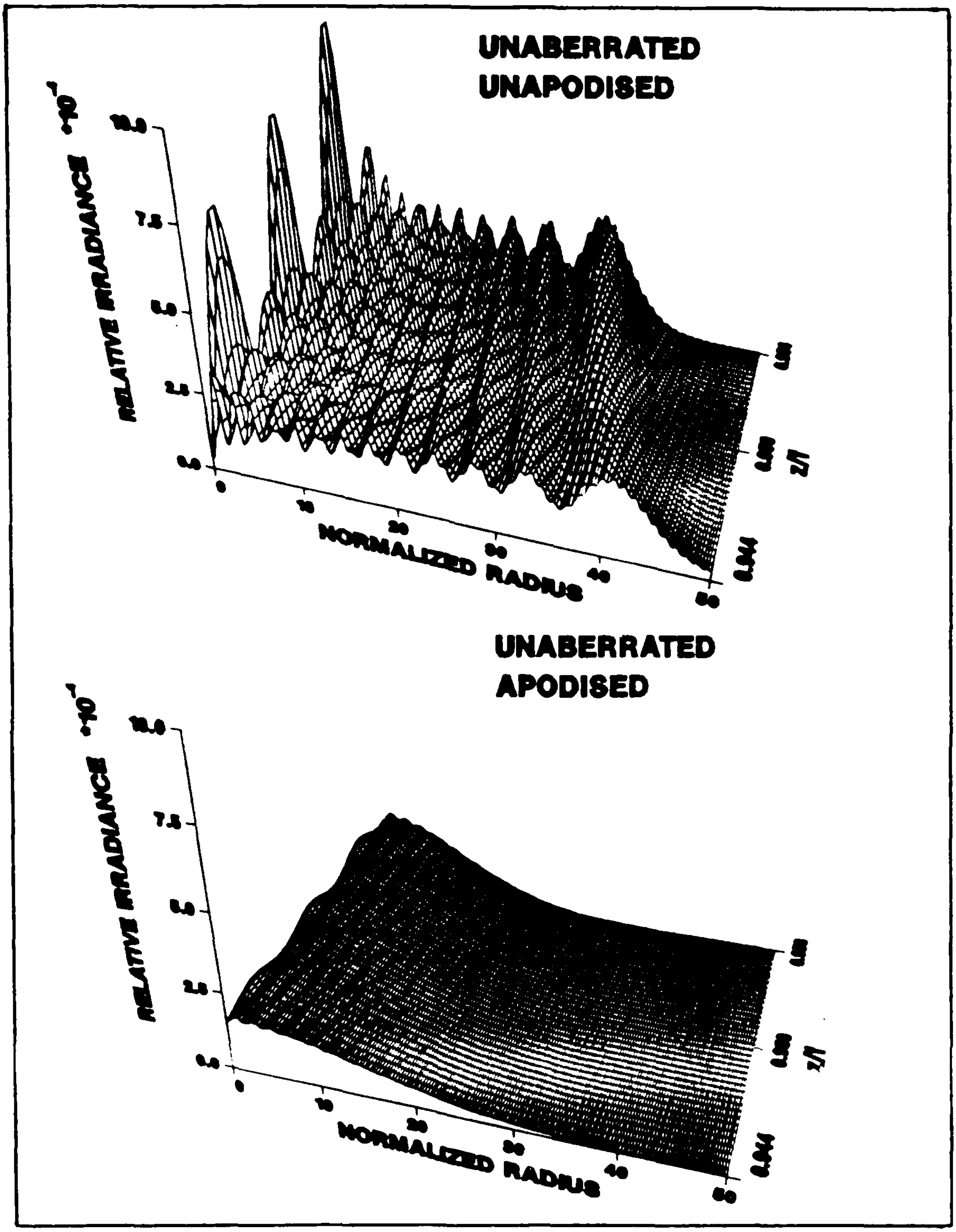

Fig. 11. Meridional Plane Irradiance in the Fresnel Region

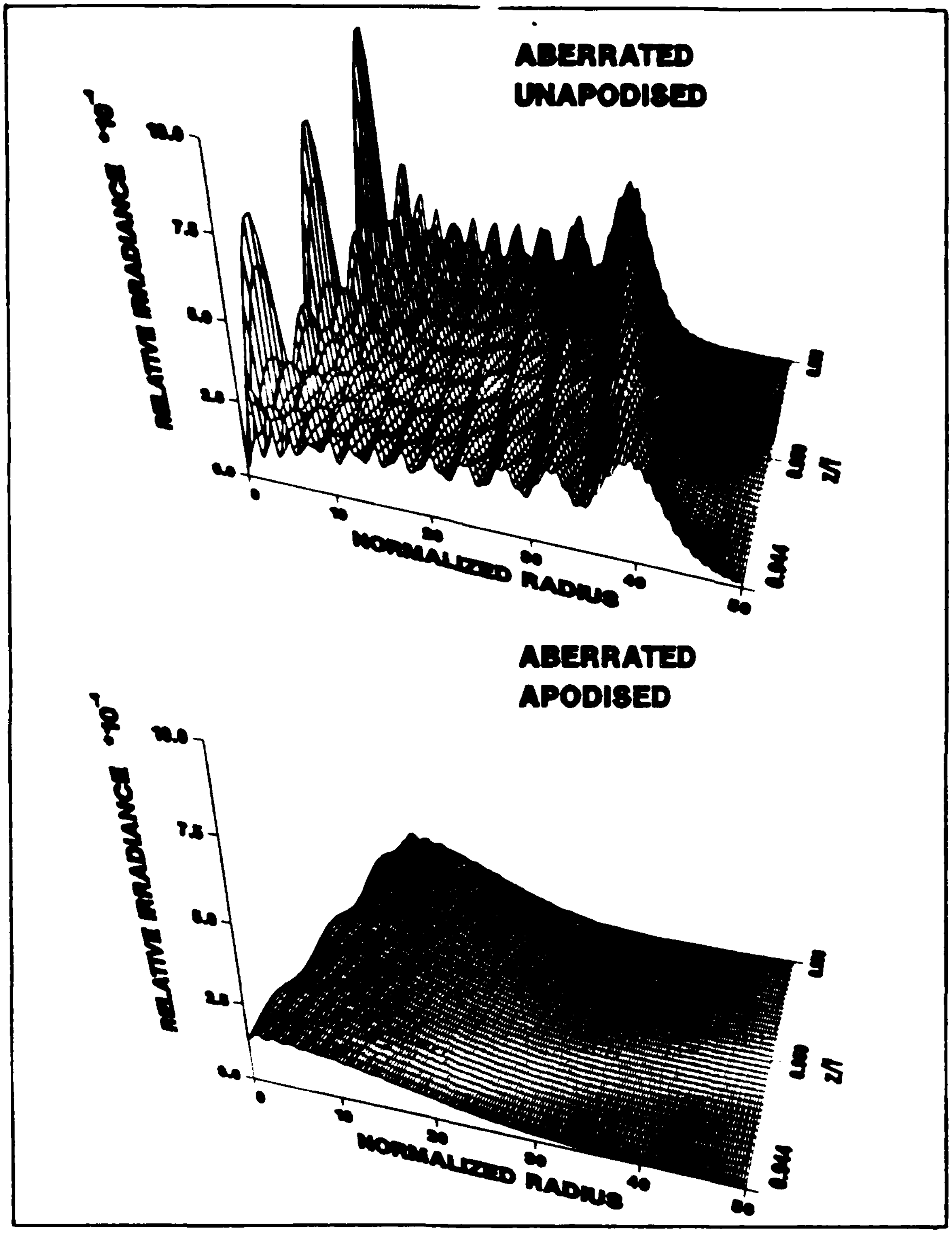

Fig. 11--Continued

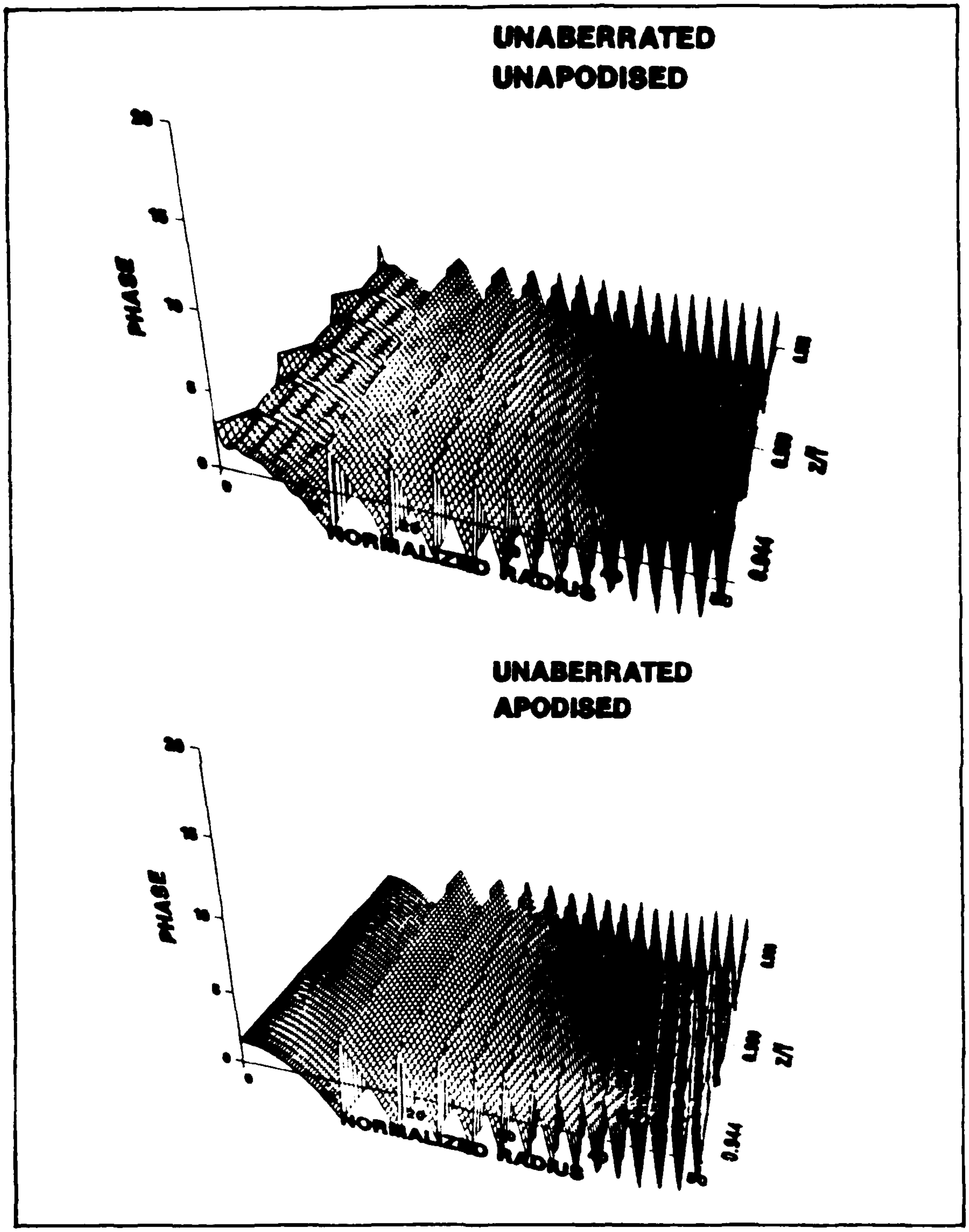

Fig. 12. Meridional Plane Phase in Radians
in the Fresnel Region

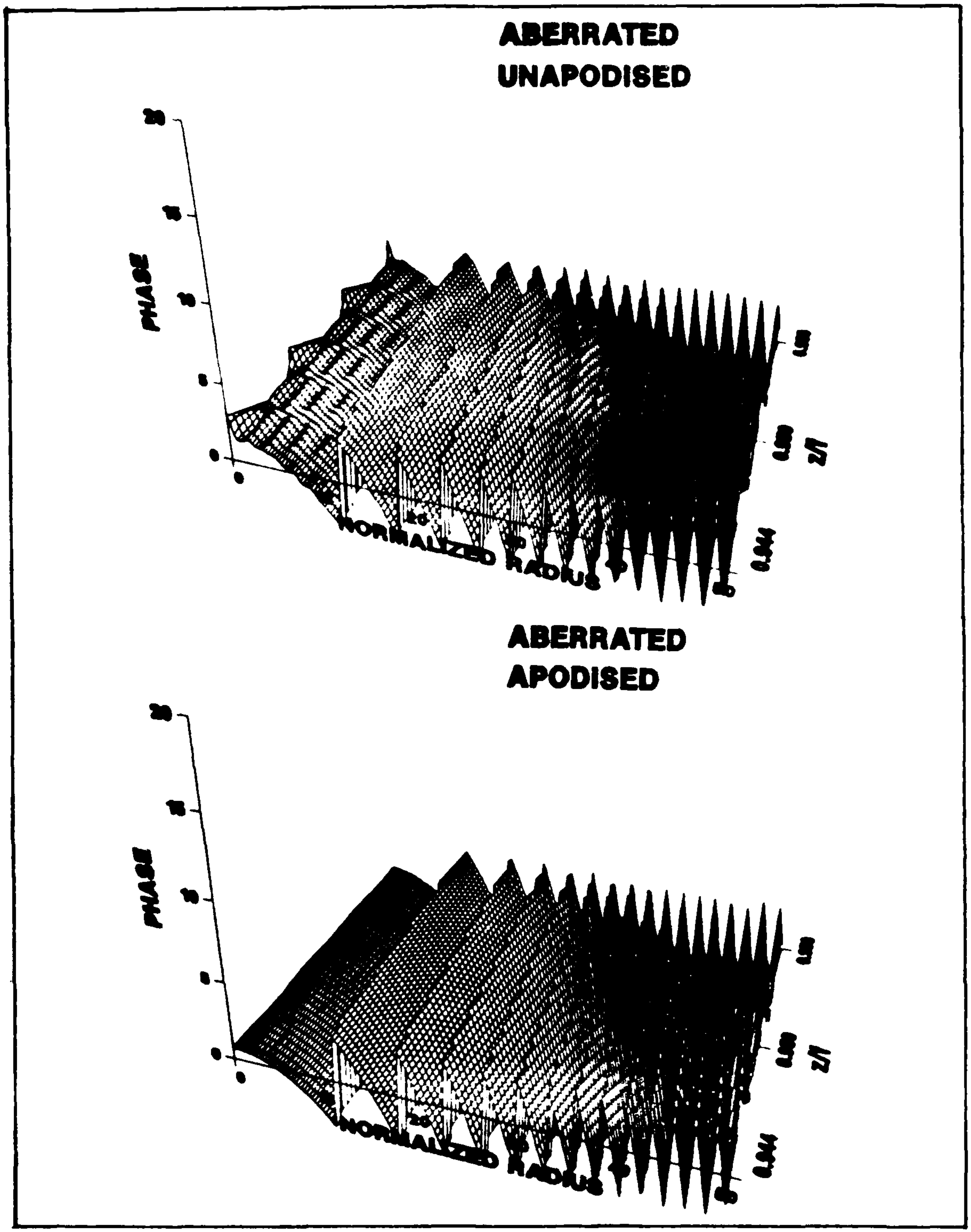

Fig. 12--Continued

IV. Experimental Results

Experimentation was undertaken to study the effects of apodisation and to test the theoretical predictions. The cross-sectional planes studied were at the first and twelfth minima on the optical axis from the focus toward the aperture. In the unaberrated and unapodised system, these minima correspond to zeros in irradiance and lie in the meridional plots of the previous section. The system used experimentally consisted of a He-Ne laser producing a coherent beam with a wavelength of 632.8 nm. The aperture diameter was set at 1.3335 cm (0.525 inches) and the system was set up to have an f-number of 12. An apodiser, designed and constructed by Mills (21:178) and having the characteristics given in Figure 3 was used. The list of experimental equipment is in Table II and was arranged as depicted in Figure 13.

The system was aligned using the techniques of Taylor and Thompson (24:440) and Mills (21:111-115). Detailed explanations of alignment techniques are explained in these sources and are not covered here.

Measurements of Aberration

The measurement of the amount of spherical aberration present within the system was accomplished by use of a Smartt Point Diffraction Interferometer (PDI) (23). This

TABLE II

EXPERIMENTAL EQUIPMENT

Equipment	Model or Type	Source	Description
Laser	He-Ne		2mW-linearly polarized
Absorbing Filter	945A	Newport	Variable values
Mirrors	GM-2	Newport	5cm diameter, pyrex
Spatial Filter	LPSF-100	Jodom	10X microscope objective 10 μm pinhole
Lens 1		Aegers	80mm diam. f = 495mm
Lens 2		Aegers	54mm diam. f = 580mm
Iris	ID-1.5	Newport	18 curved leaves
Apodiser	#6	Mills	As in Figure 3
PDI		Ealing	Smartt Point Diffraction Interferometer
Camera	4x5	Graphic	Poloroid Type
Camera	K1000	Pentax	35mm used without lens
Film	57	Polaroid	3000 ASA, Print
Film	Ektachrome	Kodak	100 ASA, Slide

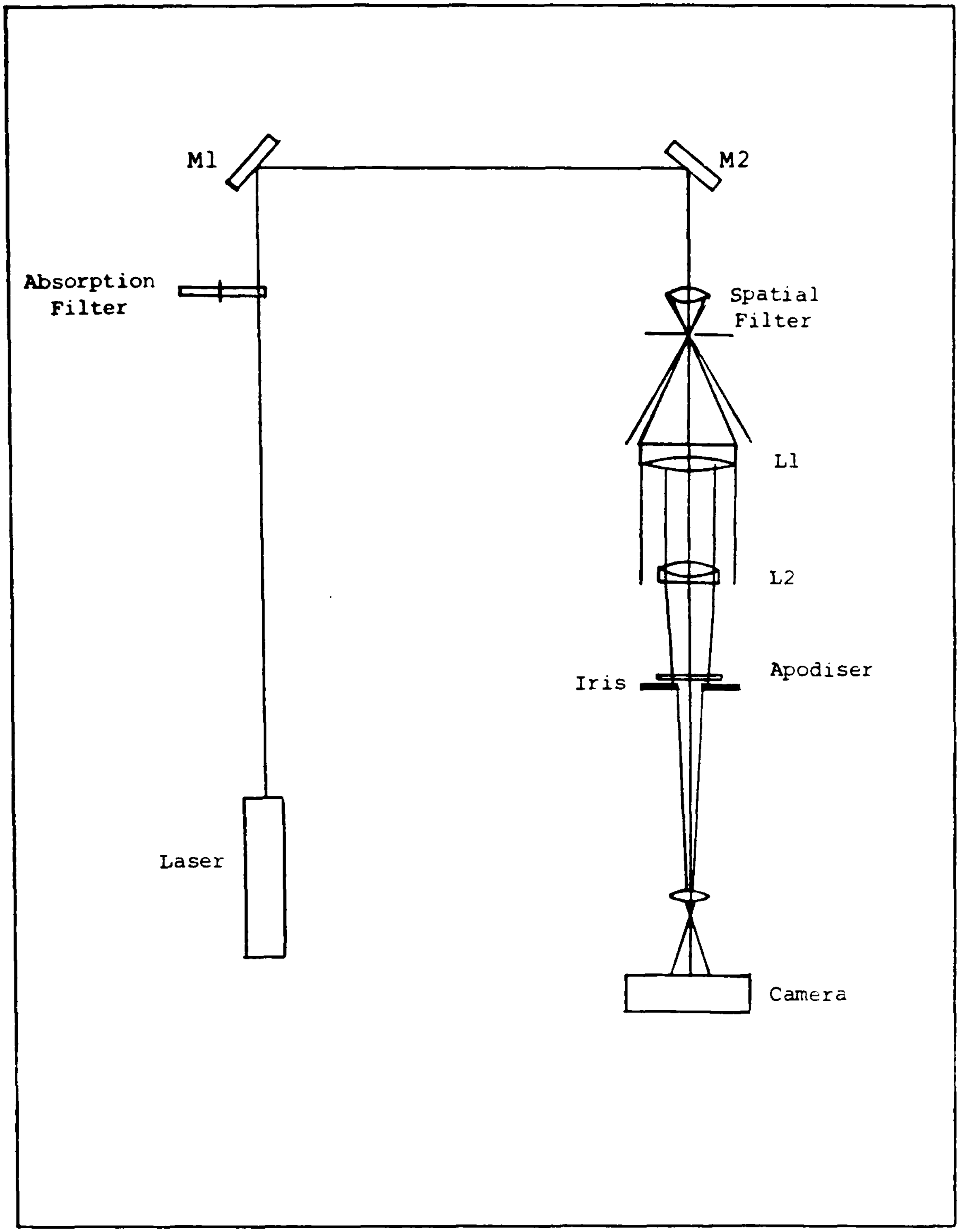

Fig. 13. Experimental Arrangement

was placed at the focus and allowed the beam to pass through the PDI while a nonaberrated expanding wave front was produced in the focal plane. The pattern resulting from the interference of the two waves indicated the amount of aberration present. Aberrations could be induced within the system by reversing Lens L2 from its depiction in Figure 13. Since L1 and L2 are achromatic doublets, they produce a minimum amount of spherical aberration when the infinite conjugate sides of each lens face one another. When L2 is reversed a maximum amount of negative spherical aberration is created. Zero aberration was measured when the conjugates faced each other. The f/12 aperture on the PDI was used and gives the sharpest contrast in fringes when used with an f/12 system. The amount of aberration was measured by comparing photographs of the image of the aperture when fully open and when set at 0.525 inches. The center of the first dark fringe occurs when the interfering waves are out of phase by a half wavelength. Since spherical aberration increases radially as ρ^4, the aberration is greater when the aperture iris is fully opened. When the iris is set at the desired aperture size, the beam is truncated and the amount of aberration is reduced. The two photographs were then compared with a simple plot of ρ^4 on an x-y plot. The first maximum corresponds to one wave of aberration. The truncated aberration then simply is taken from the ρ^4 plot as in Figure 14. The aberration was

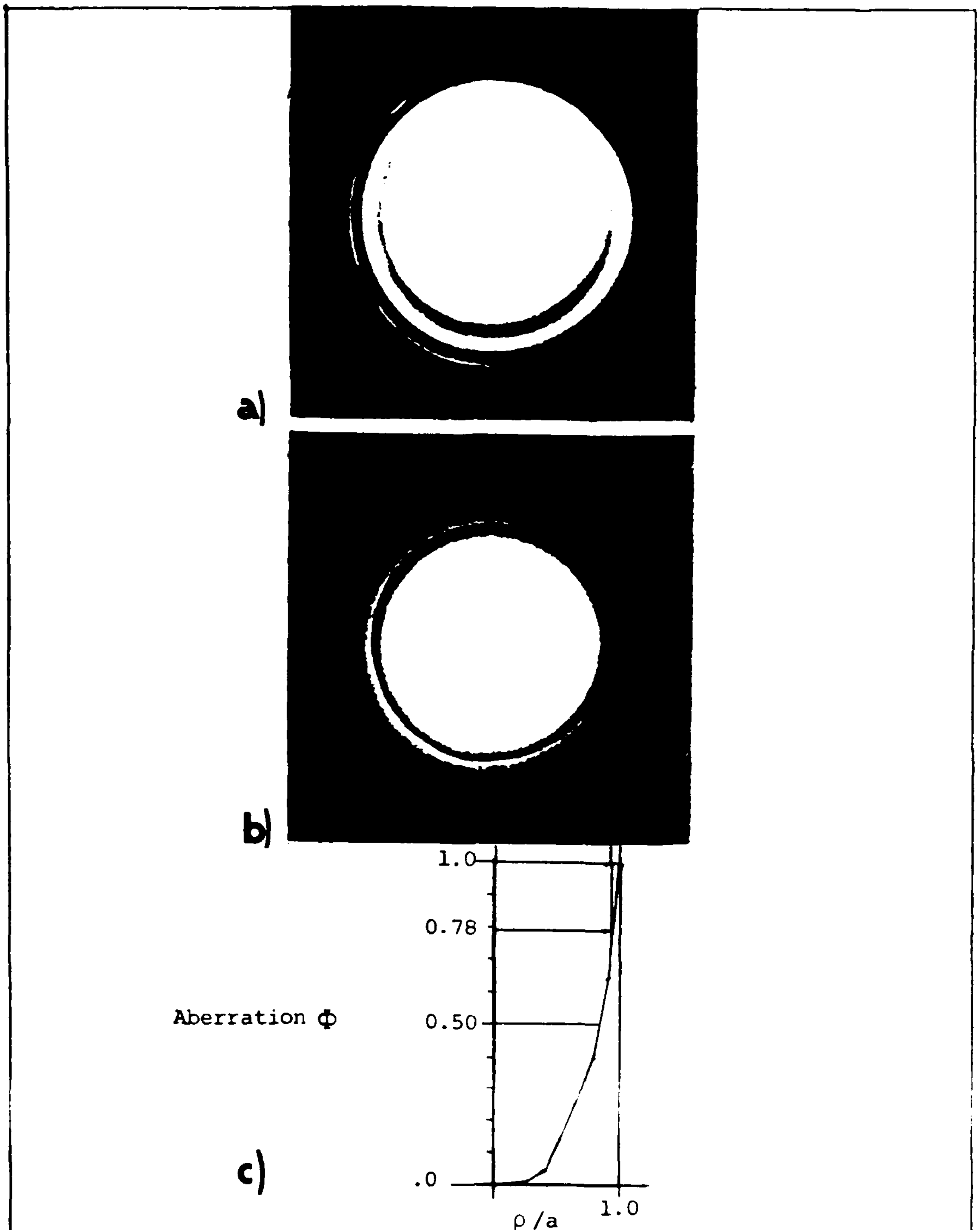

Fig. 14. Measurement of Aberration: a) Open Aperture Interferogram; b) Truncated Aperture Interferogram, Aberration (ρ^4) vs ρ

measured at -0.78 ± 0.05. The value of -0.8 was used in the running of all the computer codes in which a non-zero value for spherical aberration was needed.

The First On-axis Minimum

Comparisons of the four cases under study at the first on-axis minimum are in Figures 15a-d, along with the corresponding computer predictions for the radial irradiance.

The alignment in this region is extremely sensitive making the production of a perfectly symmetric diffraction pattern quite difficult. This could be caused by other existing low amplitude aberrations produced by the test lens L2. These aberrations were not large enough to be measured by the PDI using the technique just described.

The results of the experimental work shows qualitatively good comparison with the theoretical predictions. The unaberrated on-axis zero is lost due to the loss of edge diffraction by the aperture when the apodiser is in place. Without the apodiser, the aberrated system produces a minimum at the same axial point, though the irradiance is greater than zero. In all cases, the apodisation is seen to dramatically reduce the diffraction ringing effect. Additionally, there is also a reduction in the irradiance amplitude.

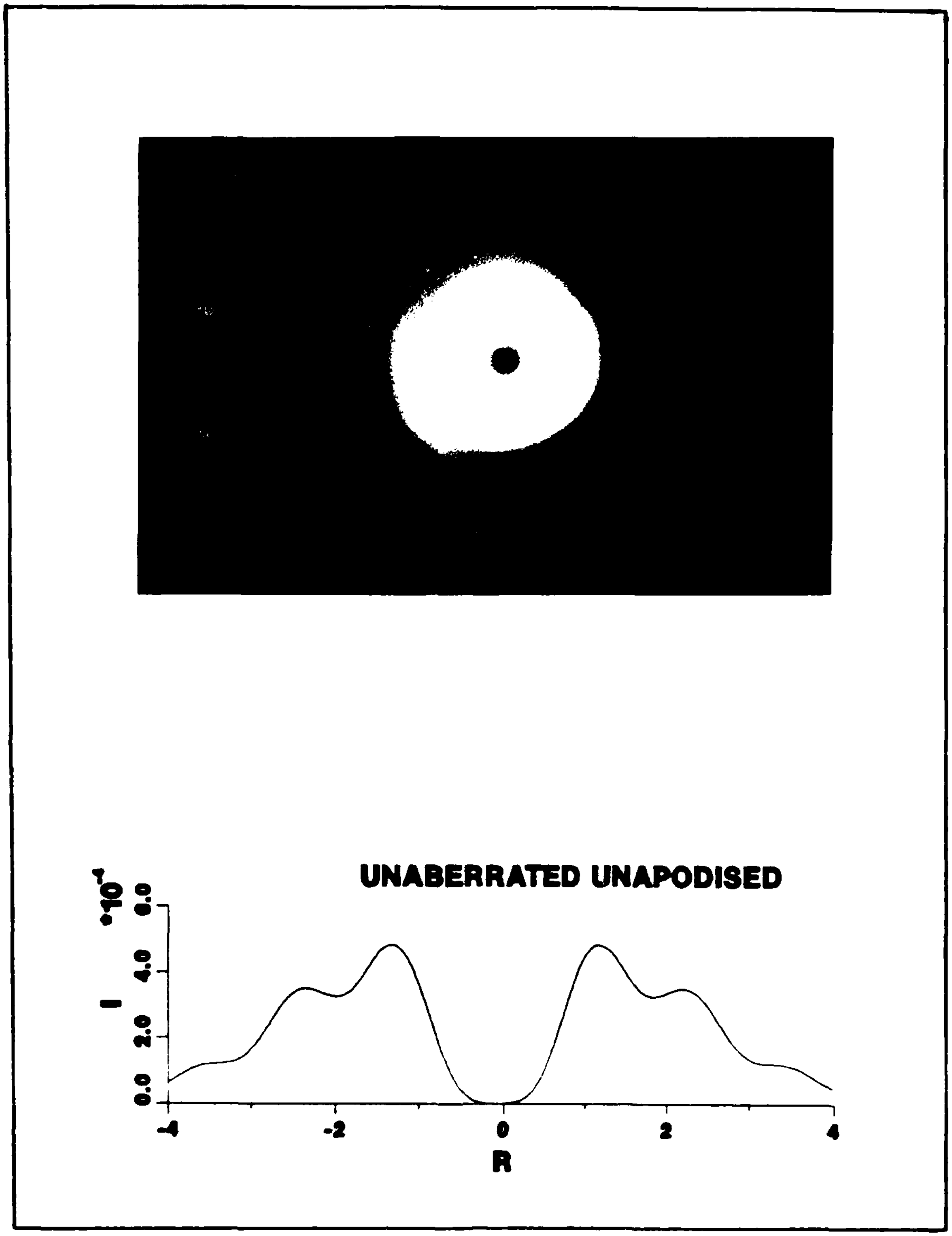

Fig. 15a. Photograph and Calculated Irradiance for the First On-axis Minimum. Case I: Unaberrated, Unapodised

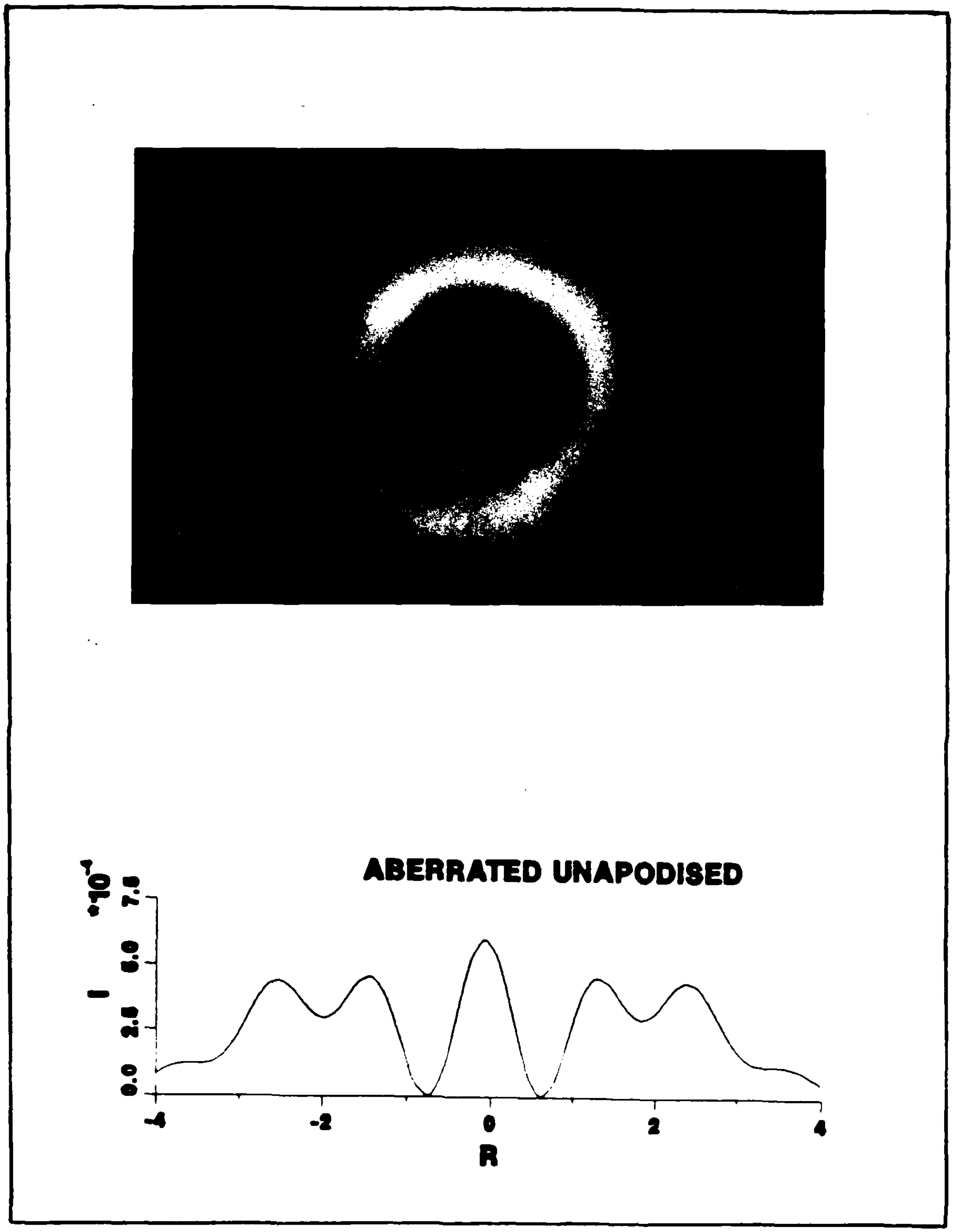

Fig. 15b. Photograph and Calculated Irradiance for the First On-axis Minimum, Case II: Aberrated, Unapodised

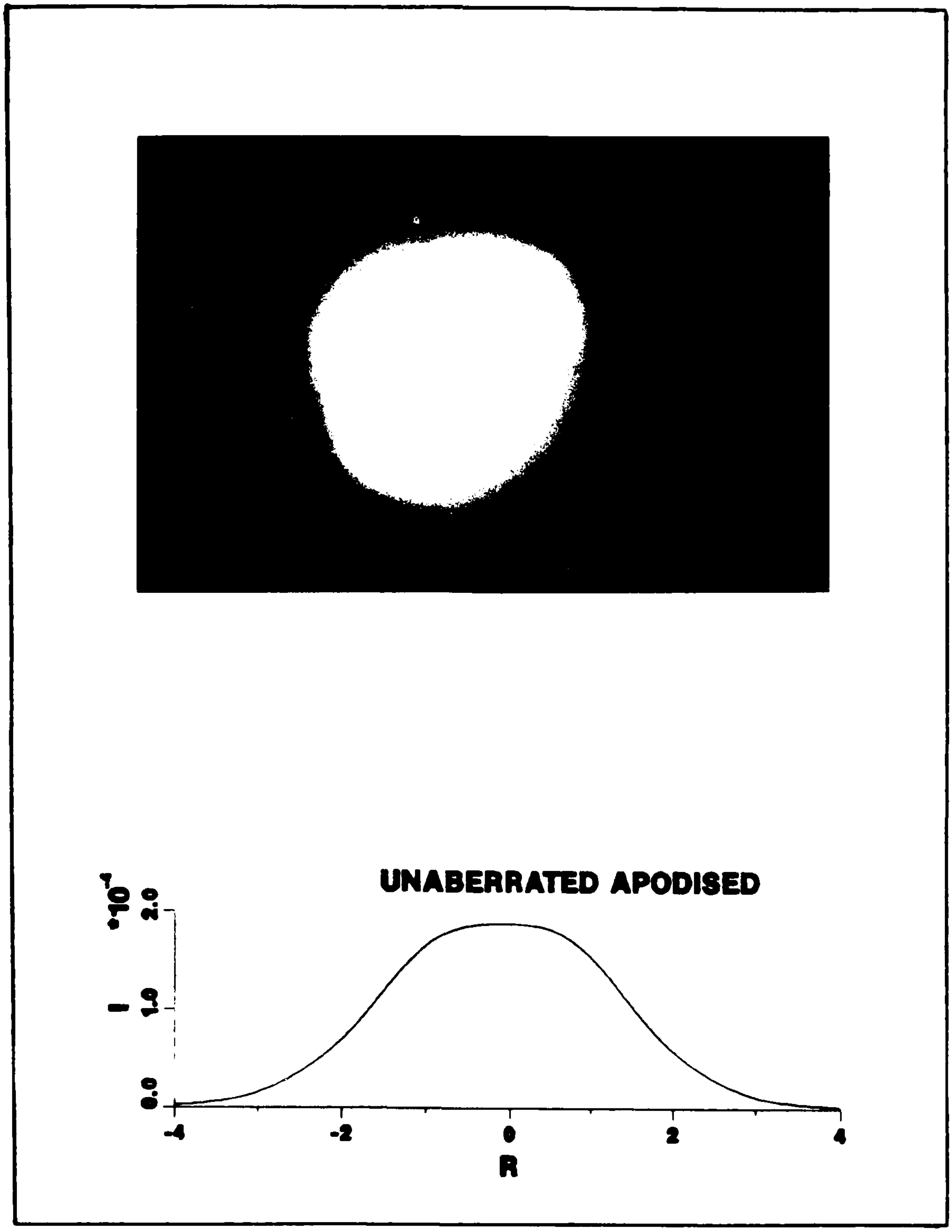

Fig. 15c. Photograph and Calculated Irradiance for the First On-axis Minimum, Case III: Unaberrated, Apodised

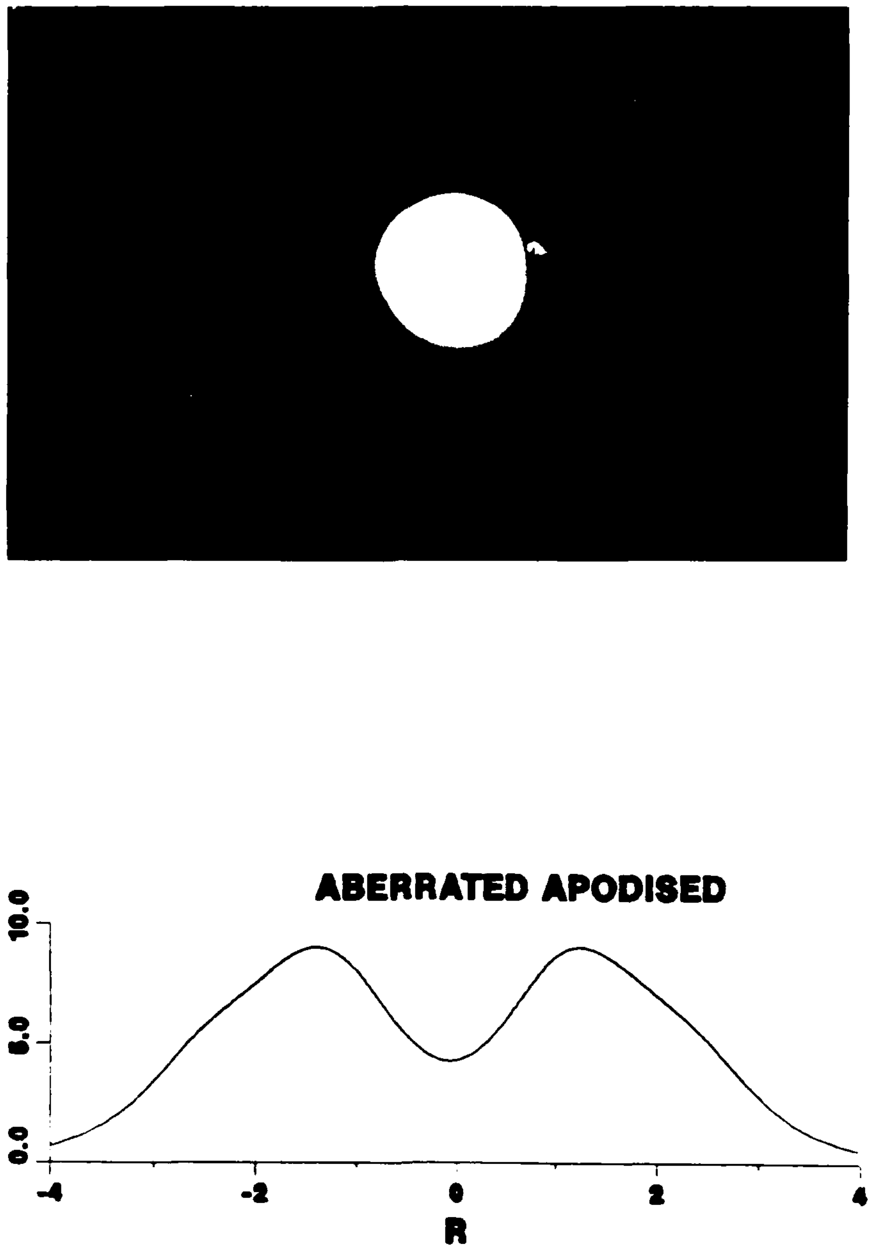

Fig. 15d. Photograph and Calculated Irradiance for the First On-axis Minimum, Case IV: Aberrated, Apodised

The Fresnel Region

The 12th on-axis minimum was photographed for all four cases. The results appear in Figures 16a-d, along with computer predictions for the radial irradiance.

The on-axis minimum has an irradiance value of zero for both the aberrated and unaberrated systems. The radial ringing has higher peaks and lower valleys for the aberrated system which are seen as brighter and darker regions in the photograph.

The radial fine structure is clearly seen on both unapodised photographs. They show an angular dependence on this structure due to a non-circular aperture. The aperture used was an iris with 18 curved leaf edges arranged in a circular pattern. At optical wavelengths, this circular approximation is easily detected by the angular dependence of the fine structure. Additionally, the region near the optical axis shows angular dependence. This is also due to the non-circular aperture.

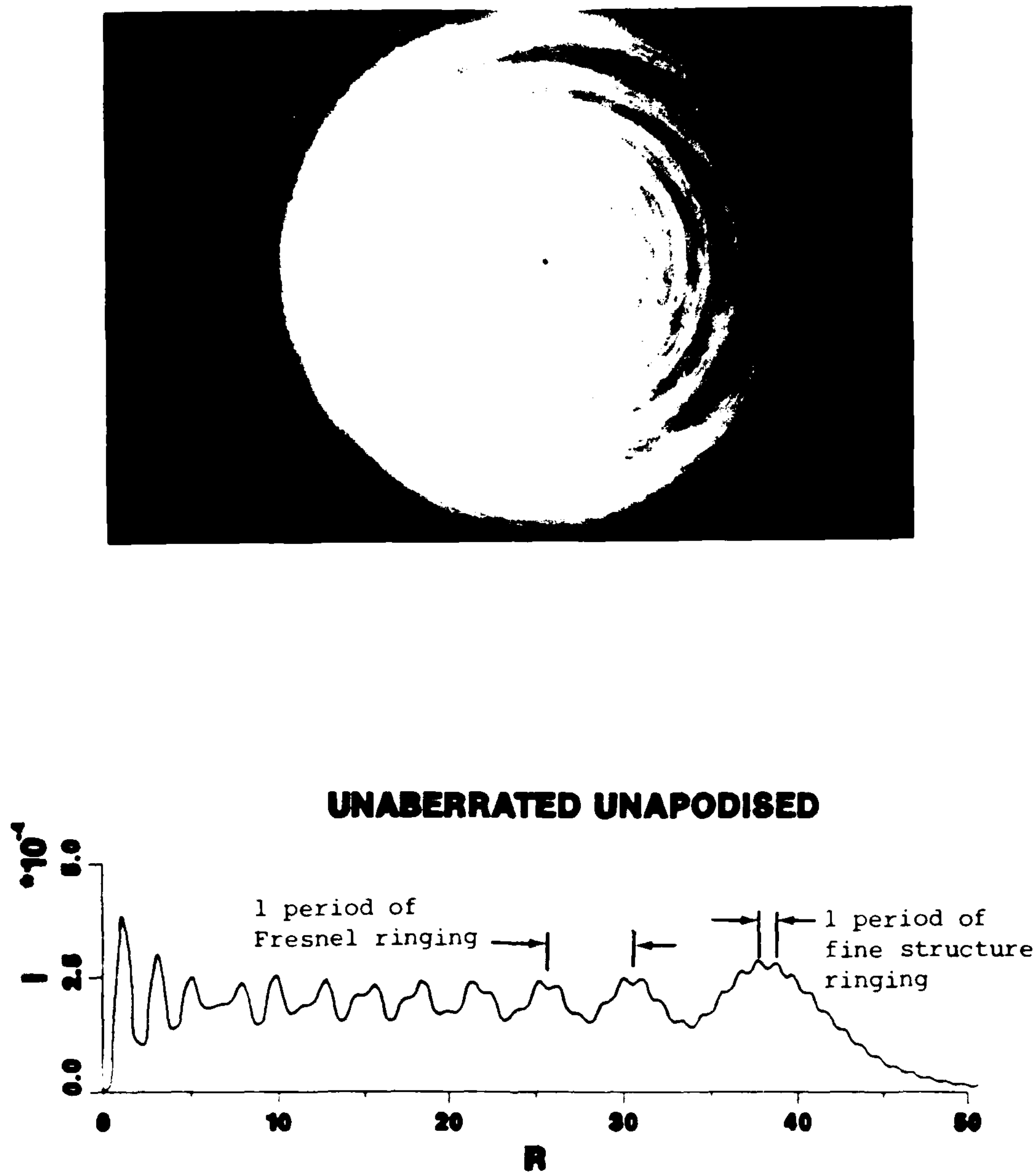

Fig. 16a. Photograph and Calculated Irradiance for the Twelfth On-axis Minimum, Case I: Unaberrated, Unapodised

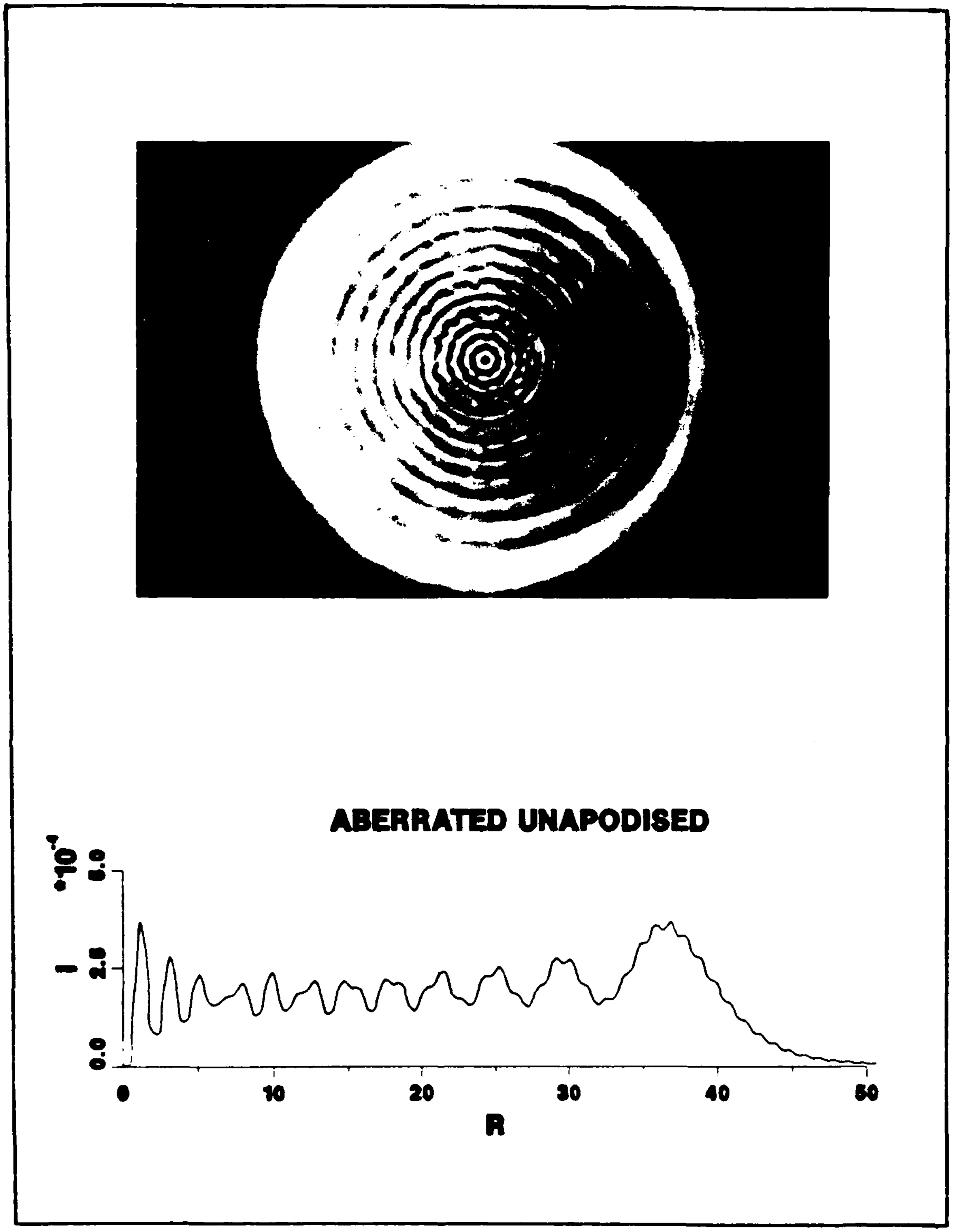

Fig. 16b. Photograph and Calculated Irradiance for the Twelfth On-axis Minimum, Case II: Aberrated, Unapodised

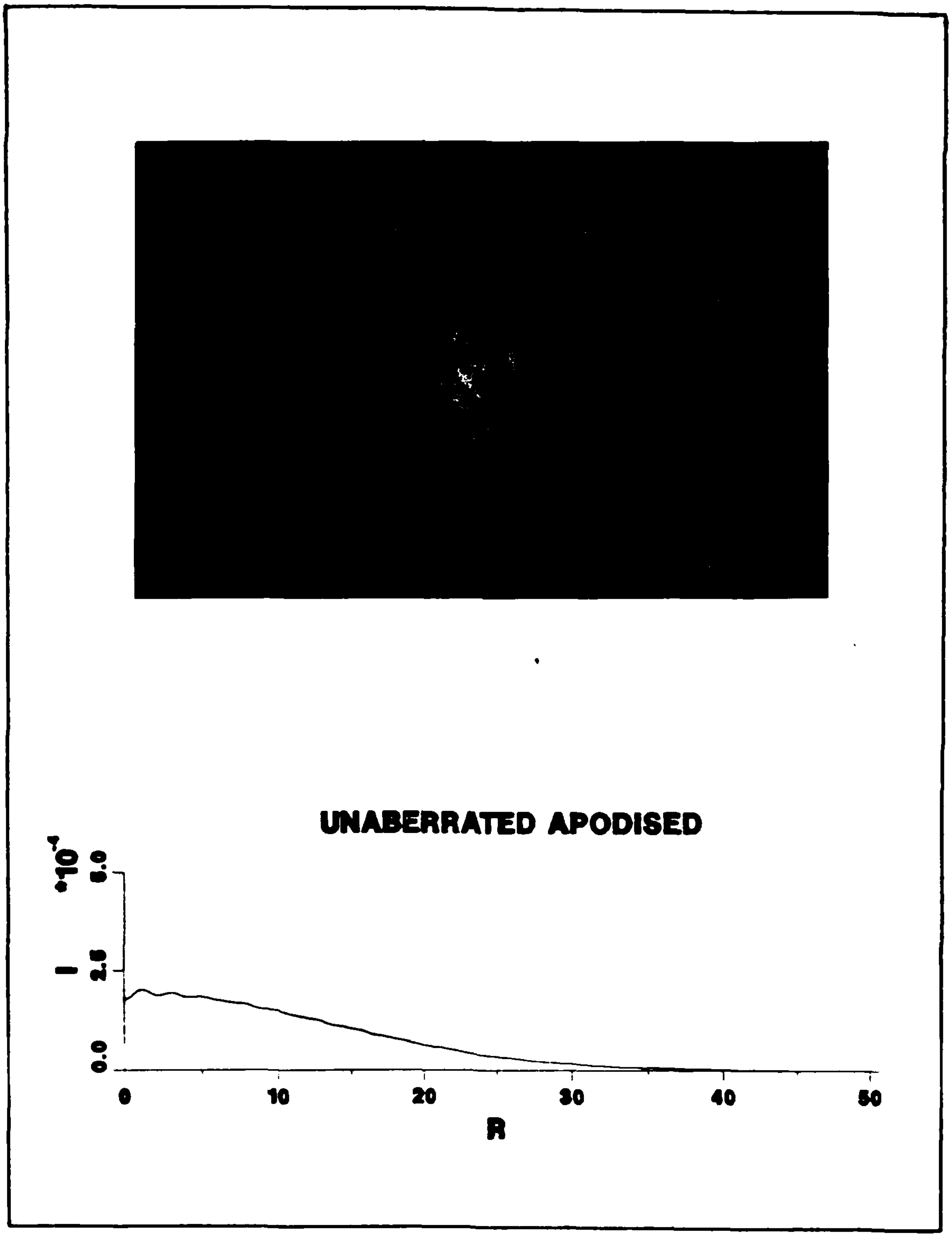

Fig. 16c. Photograph and Calculated Irradiance for the Twelfth On-axis Minimum, Case III: Unaberrated, Apodised

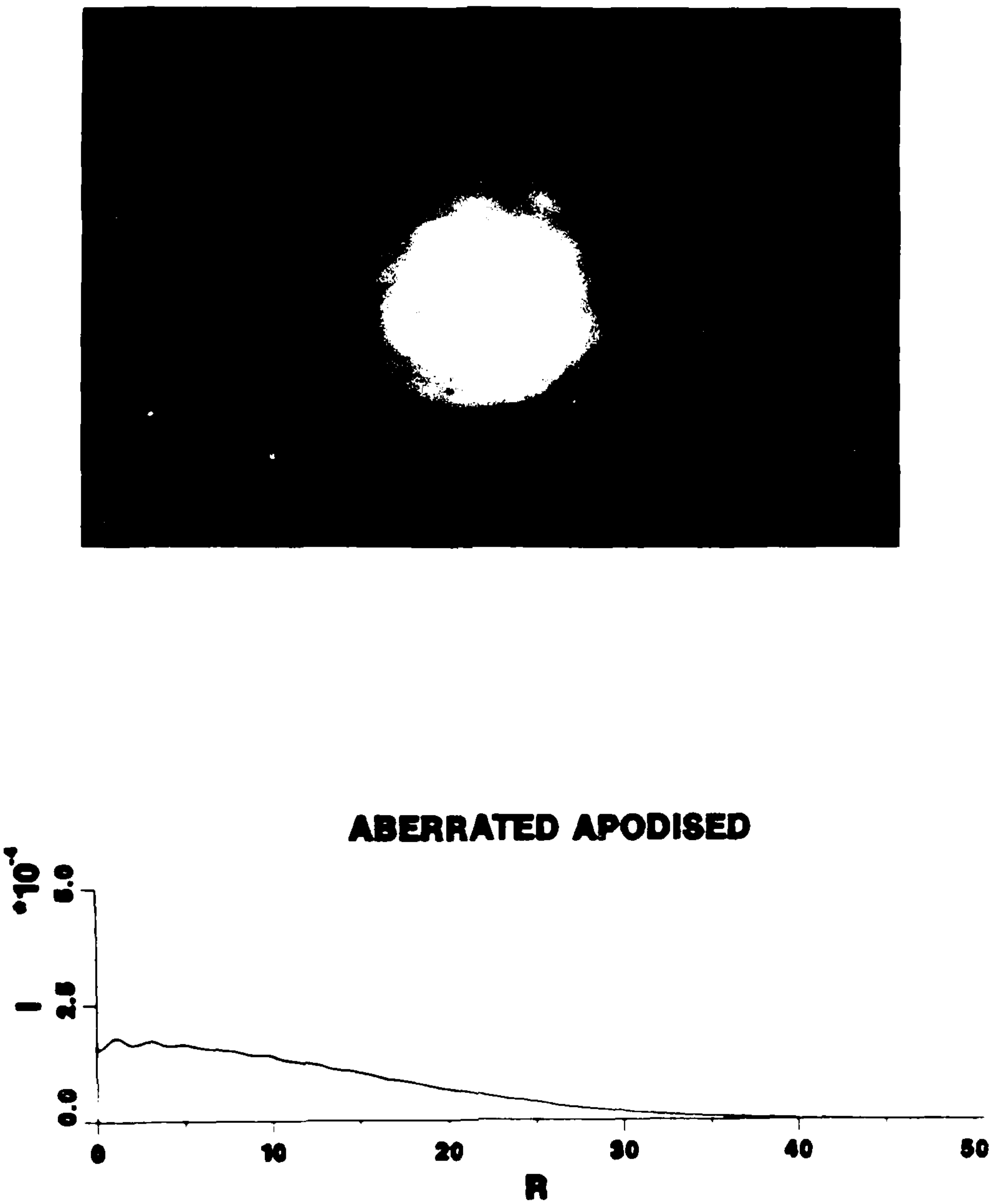

Fig. 16d. Photograph and Calculated Irradiance for the Twelfth On-axis Minimum, Case IV: Aberrated, Apodised

V. Conclusions

The theoretical predictions and experimental evidence clearly demonstrate that diffraction effects are substantially reduced when an aperture is apodised. The ringing phenomenon is completely attenuated in the unaberrated case and substantially reduced in the aberrated case. Also, the irradiance is also reduced in all cases of apodisation.

Additional conclusions of this research follow:

1) Scalar diffraction theory provides enough accuracy necessary to study this phenomenon,
2) The paraxial and Fresnel approximations must be carefully considered in the region of study so as to not limit the accuracy of the theory,
3) At optical frequencies and aperture sizes on the order of a centimeter, the amount of data required to model near-field irradiances becomes extremely large,
4) When spherical aberration is present, the normal Fresnel diffraction patterns are more intense in the peaks and less intense in the valleys,
5) The predicted fine structure in the Fresnel region is real and was observed experimentally; additionally, as spherical aberration increases, the fine structure decreases. This structure

has the same amplitude and frequency as that matching Young's double slit interference with slits at the aperture edges.

Areas for Further Study

The ability to model the near-field exists with the use of the codes in this study. The cross-sectional plane can be accurately predicted by the code N256.FOR which can handle all third-order aberrations and all Gaussian apodisers. The meridional plane can accurately be predicted by the use of IRAD.FOR, which can also handle non-circularly symmetric aberrations. The only limitations on the use of these codes is the computer hardware and the regions where the paraxial and Fresnel approximations maintain good accuracy. With optical frequencies and large f-numbers this is a significant portion of the Fresnel region.

This study should be continued in depth with the study of the other third-order aberrations, though this would be more difficult experimentally. Additionally, this study should be repeated with lasers of high energy.

Also, a more complete study of phase should be made. The treatment of phase incorporated in this study is only a cursory treatment and it should be investigated more thoroughly.

Appendix: Computer Codes

Several computer codes were written for this thesis of which three are included in the appendix. These codes include the most important programming techniques employed. The plots in the body of the thesis were drawn with the software package DISSPLA (6) and printed on a laser plotter.

```
      PROGRAM N256
C
C     THIS PROGRAM CALCULATES THE PHASE. MODULUS AND
C    INTENSITY OF THE TWO-DIMENSIONAL IMAGE OF AN
C    ON-AXIS POINT SOURCE THROUGH AN OPTICAL
C    SYSTEM WITH ARBITRARY ABERRATIONS AND
C    APODISATION INCLUDING THE NEAR FIELD
C
C

      INTEGER IWK(2000).IA1.IA2.N1,N2,N3,IJOB
      INTEGER S2.S
      REAL RWK(2000)
      REAL P(256.256).M(256.256).E(256).INT(256.256)
      COMPLEX A(256.256).CWK(256).B(256.256).C(256)
      COMPLEX D(256)

      WRITE (*.*) 'INPUT S:'
      READ (*.*) S

      WRITE (*.*) 'INPUT RADIUS MULTIPLIER:'
      READ (*,*) RM
      WRITE (*.*) 'NORMALIZE? (1.0 = YES, 0.0 = NO):'
      READ (*.*) FLAG
      IF (FLAG .NE. 1.0) THEN
         FLAG = 0.0
         WRITE (*.*) 'Unnormalized'
      END IF

C
        OPEN(UNIT=22.STATUS='NEW',FILE='PH.DAT')
        OPEN(UNIT=23.STATUS='NEW',FILE='MOD.DAT')
        OPEN(UNIT=24.STATUS='NEW',FILE='INT.DAT')
        OPEN(UNIT=25.STATUS='NEW',FILE='BB.DAT')

       S2 = S / 2

C
C    READ PARAMETER VALUES FROM MIC FILE
C
C
C      READ(5.20)N
       N = 256
C      READ(5.40)A20
       A20 = 0.
       WRITE(*.*)'A21:'
       READ(*.*)A21
C      A21 = 0.01
C      READ(5.40)A22
       A22 = 0.
C      READ(5.40)A31
```

```
          A31 = 0.
C         READ(5,40)A32
          A32 = 0.
         WRITE (*,*) 'INPUT A42:'
         READ(*,*)A42
         WRITE (*,*) 'INPUT GG:'
         READ(*,*)GG
         WRITE(*,*) 'INPUT z/f:'
         READ(*,*) FRAC
C        WRITE(5,*) 'INPUT APERTURE FRESNEL NO.: '
C        READ (5,*) FN
         FN = 439.021
         PI = 4.*ATAN(1.0)

C         20 FORMAT(I4)
  40         FORMAT(1PE11.4)
  41         FORMAT(I4,3X,I4,3X,1PE11.4,3X,1PE11.4)
  42         FORMAT(I4,3X,I4,3X,1PE11.4)
  43         FORMAT(3(2X,I4),5(3X,F9.4))
  44         FORMAT(I4,3X,1PE11.4,3X,1PE11.4)
C
C          N=NUMBER OF SAMPLE POINTS IN ONE DIMENSION
C        A20=45 deg ASTIGMATISM
C        A21=FOCAL SHIFT
C        A22=0 deg ASTIGMATISM
C        A31=X COMA
C        A32=Y COMA
C        A42=SPHERICAL
C         GG=WIDTH OF GAUSSIAN
C        FRAC=PERCENTAGE OF FOCAL LENGTH IN NEAR FIELD
C         FL=FOCAL LENGTH IN APERTURE DIAMETERS

C
C
C  CIRCULAR APERTURE WITH VARIABLE TRANSMITTANCE
C  AND ABERRATIONS
C

          R1 = 17.0*RM
          R2 = 18.0*RM
          R3 = 16.0*RM


          DO 220 I=1,N
             DO 200 J=1,N
               RAD=SQRT((I - (R2+0.5))**2+(J-(R2+0.5))**2)
               X=(I-(R2+0.5))/R1
               Y=(J-(R2+0.5))/R1
C       CALCULATE CONTRIBUTIONS OF THIRD ORDER
C       ABERRATIONS
C       USING ZERNIKE MONOMIAL REPRESENTATION
               ARG20=A20*2.*X*Y
```

```
            ARG21=A21*(-1+2.*Y*Y+2.*X*X)/2.
            ARG22=A22*(Y*Y-X*X)
            ARG31=A31*(-2.*X+3.*X*Y*Y+3.*X**3)/3.
            ARG32=A32*(-2.*Y+3.*Y**3+3.*X*X*Y)/3.
            ARG42A = A42*( 1. - 6.*Y*Y - 6.*X*X + 6.*Y**4 )
            ARG42  = ARG42A + ( 12.*X*X*Y*Y + 6.*X**4 )*A42
            ARG42  = ARG42/6.
            ARG1=(ARG20+ARG21+ARG22+ARG31+ARG32+ARG42)*2.*PI
C       CALCULATE CONTRIBUTIONS OF VARIOUS APODISERS
C       GAUSSIAN APODISER
C       TT=EXP(-GG*RAD*RAD/R1/R1)
C       SUPERGAUSSIAN APODISER
            P=1.
            R = RAD / R1
            TT = EXP(-GG * R**2)
C  CALCULATE ARG2. THE NEAR-FIELD CONTRIBUTION
            ARG2 = PI * FN * (1 - FRAC) / FRAC * R**2
            IF(RAD.LT.R3+0.5)GO TO 60
            IF(RAD.GT.R1+0.5)GO TO 100
            SC=-RAD+R1 + 0.5
            GO TO 80
   60       A(I.J)=CMPLX(TT*COS(ARG1+ARG2).TT*SIN(ARG1+ARG2))
            GO TO 120
   80       A(I.J)=CMPLX(SC*TT*COS(ARG1+ARG2).SC*TT*SIN(ARG1+ARG2))
            GO TO 120
  100       A(I.J)=(0..0.)
  120     CONTINUE
  210   CONTINUE
  220 CONTINUE
C         DO 230 I=1.S
C         DO 225 J=1.S
C         M(I.J)=CABS(A(I.J))
C         WRITE(24.42)I.J.M(I.J)
C 225     CONTINUE
C 230     CONTINUE
C
C  PERFORM FAST FOURIER TRANSFORM USING IMSL
C
  240 IA1=N
      IA2=N
      N1=N
      N2=N
      N3=1
      IJOB=-1
      CALL FFT3D (A.IA1.IA2,N1,N2,N3.IJOB,IWK,RWK,CWK)
C         DO 242 J=1,N
C         I=1
C         WRITE(22.41)I,J,A(I,J)
C242      CONTINUE
C
C  REDUCE SIZE OF ARRAY
```

```
C
          DO 250 I=1,S2
             DO 245 J=1,S2
                B(I,J)=A(I,J)
                B(I,S2+J)=A(I,N-S2+J)
                B(S2+I,J)=A(N-S2+I,J)
                B(S2+I,S2+J)=A(N-S2+I,N-S2+J)
245          CONTINUE
250       CONTINUE
C         DO 252 I=1,S
C            DO 251 J=1,S
C               WRITE(23,41)I,J,B(I,J)
C251         CONTINUE
C252      CONTINUE
C
C   SHIFT ZERO FREQUENCY TO ARRAY CENTER
C
          DO 260 I=1,S
             DO 255 J=1,S2
                A(I,J)=B(I,S2+1-J)
                A(I,S2+J)=B(I,S+1-J)
255          CONTINUE
260       CONTINUE
          DO 270 I=1,S2
             DO 265 J=1,S
                B(I,J)=A(S2+1-I,J)
                B(S2+I,J)=A(S+1-I,J)
265          CONTINUE
270          CONTINUE
          DO 274 J=1,S
             DO 272 I=1,S
C               TYPE 41,I,J,B(I,J)
272          CONTINUE
274       CONTINUE
C
C   FIND PHASE OF ARRAY
C
  348 DO 360 I=1,S
          DO 340 J=1,S
             AA=AIMAG(B(I,J))
             BB=REAL(B(I,J))
             IF (BB.EQ.0.00000000)BB=0.000001
             P(I,J)=ATAN2(AA,BB)
C            WRITE(25,42)I,J,P(I,J)
  340     CONTINUE
  360 CONTINUE
C
C   FIND MODULUS AND INTENSITY OF ARRAY
C
        DO 400 I=1,S
           DO 380 J=1,S
             M(I,J) =  CABS(B(I,J)) /  FRAC
             INT(I,J)=M(I,J)**2.
```

```
 380     CONTINUE
       PRINT *,'INT(S2,S2) =',INT(S2,S2)
      CENTINT = INT(S2,S2)
      CENTM   = M(S2,S2)
 400  CONTINUE
      IF (FLAG .EQ. 0.0) GOTO 401
      DO 21 I=1,S
         DO 22 J=1,S
            M(I,J)=M(I,J)/CENTM
            INT(I,J)=INT(I,J)/CENTINT
 22        CONTINUE
 21    CONTINUE
 401   CONTINUE
        DO 404 I=1,S
           DO 402 J=1,S
              WRITE(23,42)I,J,M(I,J)
              WRITE(24,42)I,J,INT(I,J)
 402       CONTINUE
 404    CONTINUE
C  WRITE CENTRAL SLICE OF INTENSITY
        DO 415 I=1,S
C          WRITE(23,44)I,M(I,S2)
           WRITE(25,44)I,INT(I,S2)
415     CONTINUE
       DL = 3.*PI/2.
       Q1 = 3.*PI/4.

C
C  REMOVE TILT FROM EACH ROW
C
        DO 420 I=1,S
          DO 410 J=2,S
            P(I,J)=P(I,J)-(J-1)*.4295
C           WRITE(23,42)I,J,P(I,J)
  410       CONTINUE
  420     CONTINUE
C


C  HANDLE PHASE JUMPS ON EACH ROW

        DO 500 I=1,S
        DEL=0.
        ICNT=0
          DO 490 J=1,S
            ICNT=ICNT+1
            P(I,J)=P(I,J)+DEL
            F1=P(I,J)
            G1=P(I,J+1)+DEL
            H1=ABS(G1-F1)
C           WRITE(22,43)I,J,ICNT,DEL,F1,G1,H1
            IF(H1.LE.Q1)GO TO 490
```

```
               IF((H1.GE.DL).AND.(G1.GT.F1))GO TO 450
               IF((H1.GE.DL).AND.(G1.LT.F1))GO TO 460
               IF(ICNT.LT.5)GO TO 411
               ICNT=4
C   DO LINEAR FIT TO LAST ICNT POINTS(B1=SLOPE)
 411            IF(ICNT.EQ.1)GO TO 431
               SXY=0.
               SX=0.
               SY=0.
               SX2=0.
               DO 421 K=1.ICNT
                 X=ICNT+1-K
                 SXY=SXY+X*F(I.J+1-K)
                 SX=SY+K
                 SY=SY+F(I.J+1-K)
                 SX2=SX2+K**2.
 421            CONTINUE
                B1=(SXY-SX*SY/ICNT)/(SX2-SX*SX/ICNT)
                GO TO 429
 431            B1=F(I.J+2)-F(I.J+1)
 429            IF((B1.LE.0.).AND.(G1.GT.F1))GO TO 430
                IF((B1.GT.0.).AND.(G1.LT.F1))GO TO 440
                ICNT=0
                GO TO 490
 430            INCT=0
                GO TO 450
 440            ICNT=0
                GO TO 460
 450            DEL=DEL-2.*PI
                GO TO 490
 460            DEL=DEL+2.*PI
 490          CONTINUE
 500        CONTINUE
C          DO 850 I=1.S
C             DO 849 J=1.S
C                  WRITE(24.42)I.J.F(I.J)
C849          CONTINUE
C850        CONTINUE
C
C   CORRECT PHASE ON ENTIRE ROWS RELATIVE TO ROW I=1

C          DO 1160 I=1.S
C             J=S2
C             WRITE(25.42)I.J.F(I.J)
C1160       CONTINUE
C   REMOVE TILT BETWEEN ROWS
           DO 1200 I=2.S
              DO 1150 J=1.S
                 F(I.J)=F(I.J)-(I-1)*.4295
 1150          CONTINUE
 1200       CONTINUE
C          DO 1210 I=1.S
```

```
C             J=S2
C             WRITE(22.42)I.J.F(I.J)
C1210      CONTINUE
C
C   HANDLE PHASE JUMPS BETWEEN EACH ROW
C
           DEL=0.
           ICNT=0
           DO 1500 I=1.S
              ICNT=ICNT+1
              DO 1510 J=1.S
              F(I.J)=F(I.J)+DEL
 1510       CONTINUE
           J=S2
           F1=F(I.J)
            G1=F(I+1.J)+DEL
            H1=ABS(G1-F1)
C           WRITE(24.47)I.J.ICNT.DEL.F1.G1.H1
           IF(H1.LE.Q1)GO TO 1500
           IF((H1.GE.DL).AND.(G1.GT.F1))GO TO 1450
           IF((H1.GE.DL).AND.(G1.LT.F1))GO TO 1460
           IF(ICNT.LT.4)GO TO 1411
           ICNT=3
C   DO LINEAR FIT TO LAST ICNT POINTS
 1411      IF(ICNT.EQ.1)GO TO 1426
           SXY=0.
           SX=0.
           SY=0.
           SX2=0.
           DO 1421 K=1.ICNT
             X=ICNT+1-K
             SXY=SXY+X*F(I+1-K.J)
             SX=SX+K
             SY=SY+F(I+1-K.J)
             SX2=SX2+K**2.
 1421      CONTINUE
           B1=(SXY-SX*SY/ICNT)/(SX2-SX*SX/ICNT)
           GO TO 1427
 1426      B1=F(I+2.J)-F(I+1.J)
 1427      IF((B1.LE.0.).AND.(G1.GT.F1))GO TO 1430
           IF((B1.GT.0.).AND.(G1.LT.F1))GO TO 1440
           ICNT=0
           GO TO 1500
 1430      ICNT=0
           GO TO 1450
 1440      ICNT=0
           GO TO 1460
 1450      DEL=DEL-2.*PI
           GO TO 1500
 1460      DEL=DEL+2.*PI
 1500      CONTINUE
           DO 2470 J=1.S
              I=S2
C            WRITE(25.42)I,J.F(I.J)
 2470      CONTINUE
C   CENTER PHASE AROUND ZERO VALUE
```

```
         DO 2501 I=1,S
          DO 2491 J=1,S
                P(I,J)=P(I,J)-9.
                WRITE(22,42)I,J,P(I,J)
 2491         CONTINUE
 2501       CONTINUE


C  WFITE CENTRAL SLICES OF MODULUS AND FHASE

C        I=62
C        DO 2550 J=1,S
C            WRITE(22,44)J,P(I,J)
C            WRITE(23,44)J,M(I,J)
C2550     CONTINUE
           CLOSE(UNIT=22)
          CLOSE(UNIT=23)
          CLOSE(UNIT=24)
          CLOSE(UNIT=25)
 11[illegible]         STOF
             END
```

```
      PROGRAM MERID.FOR
C     MERID CALCULATES THE NEARFIELD IRRADIANCE IN THE
C     MERIDIANAL PLANE. IT ASSUMS A LENS AT THE APERTURE WITH F/#
C     SET AS INPUT. ADDITIONALLY 'MERID.FOR' TAKES INTO ACCOUNT
C     THE CIRCULARLY SUMMETRIC ABERRATIONS OF DEFOCUS AND 3RD ORDE

C     SPHERICAL ABERRRATION. THE MODULUS. PHASE. AND THE OPTICAL A
IS
C     IRRADIANCE IS ALSO CALCULATED.

      PARAMETER (PI = 3.141592654)

      REAL IRR(256.256).M(256.256).PH(256.256) .MMESJO.YI(256)
      REAL YR(256)
      INTEGER I.J.K.KK
      CHARACTER*14 FILNAM1.FILNAM2.FILNAM3

C     INPUT DATA

       FLAG = 1.0
       WRITE (*.*) 'OPTICAL AXIS FILE? ("1.0" FOR YES."0.0" FOR NO

       READ (*.*) FLAG1
       WRITE (*.*) 'INPUT IRR FILENAME:'
       READ (*.2) FILNAM1
       WRITE (*.*) '       MOD FILENAME:'
       READ (*.2) FILNAM2
       WRITE (*.*) '       PH FILNAME. ("0" FOR NULL):'
       READ (*.2) FILNAM3
       IF (FILNAM3 .EQ. '0') FLAG = 0.0
     2 FORMAT(A14)
     1 FORMAT(F10.4)
       WRITE(*.*) 'INPUT A21:'
       READ (*.*) A21
C      A21 = 0.0
       WRITE(*.*) 'INPUT A42:'
       READ (*.*) A42
C      A42 = 0.0
       WRITE(*.*) 'INPUT GG:'
       READ (*.*) GG
C      GG = 0.0
       FN = 439.021
       WRITE(*.*) 'INPUT START C:'
       READ(*.*) C1
       WRITE(*.*) 'INPUT END C:'
       READ (*.*) CEND
       WRITE(*.*) 'INPUT START X:'
       READ (*.*) XO
       WRITE(*.*) 'INPUT END X:'
       READ (*.*) XEND
       WRITE(*.*) 'ARRAY ELEMENTS IN Z DIRECTION:'
       READ (*.*) LASTC
```

```
        WRITE (*,*) 'ARRAY ELEMENTS IN R DIRECTION:'
        READ (*,*) LASTR
       R1 = X0
       WRITE (*,*) 'INPUT KK, (must be an odd integer): '
    7  FORMAT(I4)
       READ(*,7) KK
       PRINT *,'KK=', KK
       DC  =  (CEND - C1)/(FLOAT(LASTC)-1.0)
       DR  = (XEND-X0) /(FLOAT(LASTR )-1.0)
       PRINT *,'DR =',DR

     4 FORMAT(1X,9X,'J=',I3)
     3 FORMAT(1X,'I=',I3)
       R  = R1
       C  = C1
       DRHO = 1.0/(FLOAT(KK)-1.0)
       PRINT *,'DRHO=',DRHO,'LASTR=',LASTR
       DO 10 I=1,LASTC
       WRITE (*,3) I
       DO 20 J=1,LASTR
           C = I*DC + C1
           R = (J-1)*DR + R1
C               WRITE (*,4) J
              RHO = 0.0
              DO 30 K=1,KK

C               * CREATING THE INTEGRAND *

C               * Aberration terms using Zernike Polynomials *

C               ARG21 corresponds to defocus
C               ARG42 corresponds to spherical aberration

                ARG21 = A21 * (2.0 * RHO**2 - 1.0)/2.0
                ARG42 = A42 * (6.0*(RHO**4 - RHO**2) + 1.0)/6.0
                ARG1 = (ARG21 + ARG42)*2.0*PI

C               * Apodisation Term *

                TT = EXP(-GG*RHO**2)

C               * Fresnel Region Term *

                ARG2 = PI * FN * (1-C)/C * RHO**2

                REA = TT*COS(ARG1+ARG2)
                AIM = TT*SIN(ARG1+ARG2)

                ARG = PI * R * RHO/C
                YR(K) = REA * RHO * MMBSJ0(ARG,IER)
                IF (IER .NE. 0) PRINT *,'IER=',IER
                YI(K) = AIM * RHO * MMBSJ0(ARG,IER)
                IF (IER .NE. 0) PRINT *,'I IER=',IER
```

```
              RHO   = RHO + DRHO
 30         CONTINUE
            ODDR = 0.0
            ODDI = 0.0
            DO 40 K=3.KK-2.2
            ODDR = ODDR + 2.0*YR(K)
            ODDI = ODDI + 2.0*YI(K)
 40         CONTINUE

            EVENR = 0.0
            EVENI = 0.0
            DO 50 K=2.KK-1.2
               EVENR = EVENR + 4.0*YR(K)
               EVENI = EVENI + 4.0*YI(K)
 50         CONTINUE

            RINT = (DRHO/3.0) * (YR(1) + EVENR + ODDR + YR(KK))
            AIINT = (DRHO/3.0) * (YI(1) + EVENI + ODDI + YI(KK))
            M(I.J) = 2.0/C   * SQRT(RINT**2 + AIINT**2)

            IRR(I.J) = M(I.J)**2
            PH(I.J) = ATAN2(AIINT.RINT)

 20      CONTINUE
 10 CONTINUE

    OPEN(UNIT=22.STATUS='NEW',FILE=FILNAM1)
    IF (FLAG1 .EQ. 1.0) OPEN(UNIT=23.STATUS='NEW',FILE='AXIS.DAT')
    OPEN(UNIT=24.STATUS='NEW',FILE=FILNAM2)
    OPEN(UNIT=25.STATUS='NEW',FILE=FILNAM3)

 44 FORMAT(I3.3X.I3.3X.1PE11.4)
    DO 60 I=1.LASTC
       DO 70 J=1.LASTR
          V = IRR(I.J)
          WRITE(22.44) I.J.V
          WRITE(24.44) I.J.M(I.J)
          IF (FLAG .EQ. 1.0) WRITE(25.44) I.J.PH(I.J)
 70      CONTINUE
 60 CONTINUE

 45 FORMAT(I3.3X.1PE11.4)
    IF (FLAG1 .EQ. 1.0) THEN
       DO 80 I=1.LASTC
          V = IRR(I.LASTR/2)
          WRITE(23.45) I.V
 80    CONTINUE
    END IF

    CLOSE(UNIT=22)
    IF (FLAG1 .EQ. 1.0) CLOSE(UNIT=23)
    CLOSE(UNIT=24)
```

```
CLOSE(UNIT=25)

END
```

```
      PROGRAM IRAD
      REAL IRR(2000),DBLIN,FL,LAMBDA,M,K
      INTEGER I,L
      EXTERNAL F,AY,BY
      COMMON GG,K,PI,L,A42,P,Q
      CHARACTER FILNAM*14

      PI = 4.0*ATAN(1.0)

C     Input Parameter Values

      WRITE (*,*) 'FILENAME:'
   13 FORMAT (A14)
      READ  (*,13) FILNAM
      WRITE (*,*) 'X START:'
      READ  (*,*)  XO
      WRITE (*,*) 'X END:'
      READ  (*,*)  XEND
      WRITE (*,*) 'ARRAY ELEMENTS:'
      READ (*,*) N
      WRITE (*,*) 'C:'
      READ  (*,*) C
      LAMBDA = 6.238E-05
      FL = 16.002
      A = 0.66675
      Z = C * FL
      WRITE (*,*) 'A42:'
      READ  (*,*)  A42
      WRITE (*,*) 'GG:'
      READ  (*,*)  GG

      DX = (XEND - XO)/(FLOAT(N)-1.0)
      X = XO

      AR = 0.0
      BR = 1.0
      WRITE(*,*)'AERR:'
      READ (*,*) AERR

      K = 2.0*PI/LAMBDA
      RRO = SQRT(Y**2 + Z**2)
      PO = K*A**2 * (RRO - FL) / (2.0 * RRO * FL)
      QO = K*A*Y/RRO
      RR = RRO
      Q  = QO
      P  = PO

   43 FORMAT(I4,3X,1PE11.4)
      OPEN (UNIT=1,STATUS='NEW',FILE=FILNAM)
```

```
      DO 10 I=1.N
         L=1
         RE = DBLIN(F.AR.BR.AY.BY.AERR.ERROR.IER)
         PRINT *.'L=',L.' RE='.RE.'ERR='.ERROR
         IF (IER .NE. 0 .AND. 65 .AND. 66) CALL CHECK(ERROR
     $ IER.I.X)
         L=2
         AI = DBLIN(F.AR.BR.AY.BY.AERR.ERROR.IER)
         IF (IER .NE. 0 .AND. 65 .AND. 66) CALL CHECK(ERROR
     $ .IER.I.X)
           PRINT *.'L=',L.' AI=',AI,' ERR='.ERROR

           M = SQRT(RE**2 + AI**2) / (2.0*PI*FL*RR) / 1.9526365E-3
           IRR(I) = M**2
           WRITE (1.43) I.IRR(I)
           PRINT *.'I= ',I.' IRR=',IRR(I)
           PRINT *.' '

           X = X + DX
           RR = SQRT(X**2 + Z**2)
           P  = K*A**2*(RR-FL)/(2.0*RR*FL)
           Q  = K*A*X/RR
10    CONTINUE
      CLOSE(UNIT=1)
      END

C       *************** Subroutines *************************

       REAL FUNCTION F(R.Y)
       REAL LAMBDA.K,PI
       COMMON GG.K.PI,L,A42.P.Q

       IF (L .EQ. 1) THEN
       F = EXP(-GG*(R*A)**2) * COS(- P*R**2 - Q*R*COS(Y) +
     $  A42*(R**4 - R**2 + 1.0/6.0)*2*PI) * R
        ELSE IF (L .EQ. 2) THEN
        F = EXP(-GG*(R*A)**2) * SIN( -P*R**2 - Q*R*SIN(Y) +
     $  A42*(R**4 - R**2 + 1.0/6.0)*2*PI) * R
        END IF

        RETURN
        END
C      ---

      SUBROUTINE CHECK (ERROR.IER,I,X)
      REAL ERROR.X
      INTEGER IER.I

      IF (IER .GT. 0) THEN
      PRINT *.'IER=',IER.' I=',I,' X=',X
      PRINT *.' ERROR =',ERROR
      END IF
```

```
RETURN
END
REAL FUNCTION AY(R)
REAL R
AY = 0.0
RETURN
END
REAL FUNCTION BY(R)
REAL R
BY = 2.0 * 4.0*ATAN(1.0)
RETURN
END
```

Bibliography

1. Avizonis, P. V. et al. "Intensity Mapping Optical Aberrations," Applied Optics, 17: 1527-1531 (15 May 1978).

2. Bachynski, M. P. and G. Bekefi. "Study of Optical Diffraction Images in Microwave Frequencies," Journal of the Optical Society of America, 47: 428-438 (May 1957).

3. Born, Max and Emil Wolf. Principles of Optics (Fifth Edition). Oxford: Pergamon Press, 1975.

4. Campbell, J. P. and L. G. De Shazer. "Near Fields of Truncated-Gaussian Apertures," Journal of the Optical Society of America, 59: 1427-1429 (November 1969).

5. Churchill, Ruel and James Ward Brown. Fourier Series and Boundary Value Problems (Third Edition). New York: McGraw-Hill, 1978.

6. DISSPLA, graphics software product. San Diego: Integrated Software Systems, 1984.

7. Farnell, G. W. "Calculated Intensity and Phase Distribution in the Image Space of a Microwave Lens," Canadian Journal of Physics, 35: 777-783 (1957).

8. Farnell, G. W. "Measured Phase Distribution in the Image Space of a Microwave Lens," Canadian Journal of Physics, 36: 935-943 (1958).

9. Farnell, G. W. "On the Axial-Phase Anomaly for Microwave Lenses," Journal of the Optical Society of America, 48: 643-647 (September 1958).

10. Goodman, Joseph W. Introduction to Fourier Optics. San Francisco: McGraw-Hill, 1968.

11. Hadley, Ronald G. "Diffraction by Apodised Apertures," IEEE Journal of Quantum Electronics, QE-10: 603-608 (August 1974).

12. Harvey, James E. and Roland V. Shack. "Aberrations of Diffracted Wave Fields," Applied Optics, 17: 3003-3009 (15 September 1978).

13. Holmes, D. A. et al. "Parametric Study of Apertured Focused Gaussian Beams," Applied Optics, 11: 556-557 (March 1972).

14. IMSL Library. Computer Mathematics and Statistics Fortran Subroutine Library. Houston: IMSL, Inc., 1984.

15. Kuzimina, N. V. et al. "Spatial Filtering of Apodised Laser Beams," Optical Spectroscopy (USSR), 51 (September 1981).

16. Lee, L. and G. W. Farnell. "Phase Singularities for Microwave Lenses with Aberrations," Canadian Journal of Physics, 36: 935-943 (1958).

17. Linfoot, E. H. and E. Wolf. "Phase Distribution near Focus in an Aberration-free Diffraction Image," Proc. Phys. Soc., B69: 623-832 (1956).

18. Mahajan, Virendra N. "Aberrated Pont-spread Functions for Rotationally Symmetric Aberrations," Applied Optics, 22: 3035-3041 (October 1983).

19. Mahajan, Virendra N. Uniform versus Gaussian Beams. The Aerospace Corporation, Los Angeles, 1985.

20. Malacara, Daniel et al. "Optical Shop Testing," edited by Daniel Malacara. New York: John Wiley and Sons, 1978.

21. Mills, James P. The Effect of Aberrations and Apodisation on the Performance of Coherent Imaging Systems. PhD Dissertation. The Institute of Optics, University of Rochester, Rochester NY, 1984.

22. Olaofe, G. Oluremi. "Diffraction by Gaussian Apertures," Journal of the Optical Society of America, 60: 1654-1657 (December 1970).

23. Smartt, R. N. and W. H. Steel. "Theory and Application of Point-Diffraction Interferometers," Proc. ICO Conference on Optical Methods in Science and Industrial Measurements, Tokyo, 1974 also, Japan Journal of Applied Physics, 14: 351-356 (1975).

24. Taylor, C. A. and B. J. Thompson. "Some Improvements in the Operation of the Optical Diffractometer," Journal of Scientific Instruments, 34: 439-447 (November 1957).

25. Thompson, Brian J. and Matthew E. Krisl. "Evaluation of Coherent Optical Systems," Photographic Science and Engineering, 21: 109-114 (May/June 1977).

VITA

Captain Daniel B. Allred was born on 22 December 1953 in Portland, Oregon. He graduated from high school in 1972 and attended Oregon State University where he received the degree of Bachelor of Science in Physics in June 1977. He received his commission in the U.S. Air Force through Officers Training School at Lackland AFB, Texas in February 1978. He then attended Undergraduate Navigator Training and received his wings in September 1978. He served as a B-52G Electronic Warfare Officer in the 441st Bombardment Squadron at Mather AFB, California and then in the 46th Bombardment Squadron at Grand Forks AFB, North Dakota until entering the School of Engineering, Air Force Institute of Technology, in August 1984.

Permanent address: 12525 SW Colt Court
Beaverton, Oregon 97005

UNCLASSIFIED

SECURITY CLASSIFICATION OF THIS PAGE

AD-A174236

REPORT DOCUMENTATION PAGE

1a. REPORT SECURITY CLASSIFICATION: UNCLASSIFIED

1b. RESTRICTIVE MARKINGS:

2a. SECURITY CLASSIFICATION AUTHORITY:

2b. DECLASSIFICATION/DOWNGRADING SCHEDULE:

3. DISTRIBUTION/AVAILABILITY OF REPORT: Approved for public release; distribution unlimited.

4. PERFORMING ORGANIZATION REPORT NUMBER(S): AFIT/GNE/ENP/86M-1

5. MONITORING ORGANIZATION REPORT NUMBER(S):

6a. NAME OF PERFORMING ORGANIZATION: School of Engineering

6b. OFFICE SYMBOL (If applicable): AFIT/EN

7a. NAME OF MONITORING ORGANIZATION:

6c. ADDRESS (City, State and ZIP Code): Air Force Institute of Technology, Wright-Patterson AFB, Ohio 45433

7b. ADDRESS (City, State and ZIP Code):

8a. NAME OF FUNDING/SPONSORING ORGANIZATION:

8b. OFFICE SYMBOL (If applicable):

9. PROCUREMENT INSTRUMENT IDENTIFICATION NUMBER:

8c. ADDRESS (City, State and ZIP Code):

10. SOURCE OF FUNDING NOS.

PROGRAM ELEMENT NO.	PROJECT NO.	TASK NO.	WORK UNIT NO.

11. TITLE (Include Security Classification): See Box 19

12. PERSONAL AUTHOR(S): Daniel B. Allred, B.S., Capt, USAF

13a. TYPE OF REPORT: Thesis

13b. TIME COVERED: FROM ______ TO ______

14. DATE OF REPORT (Yr., Mo., Day): 1986 March

15. PAGE COUNT: 87

16. SUPPLEMENTARY NOTATION:

17. COSATI CODES

FIELD	GROUP	SUB. GR.
20	06	
07	07	

18. SUBJECT TERMS (Continue on reverse if necessary and identify by block number): Diffraction Analysis, Apodiser, Near-Field, Fresnel Diffraction, Aberration, Optical Analysis

19. ABSTRACT (Continue on reverse if necessary and identify by block number)

Title: The Near-Field Effects of Apodisation on Coherent Aberrated Optical Systems

Thesis Chairman: James P. Mills, Major, USAF

20. DISTRIBUTION/AVAILABILITY OF ABSTRACT: UNCLASSIFIED/UNLIMITED ☒ SAME AS RPT. ☐ DTIC USERS ☐

21. ABSTRACT SECURITY CLASSIFICATION: UNCLASSIFIED

22a. NAME OF RESPONSIBLE INDIVIDUAL: James P. Mills, Major, USAF

22b. TELEPHONE NUMBER (Include Area Code): 513-255-2012

22c. OFFICE SYMBOL: AFIT/PH

DD FORM 1473, 83 APR — EDITION OF 1 JAN 73 IS OBSOLETE.

UNCLASSIFIED

SECURITY CLASSIFICATION OF THIS PAGE

The effects of Gaussian apodisation with -0.8 waves of spherical aberration on a coherent optical system was examined. The area of study was in the near-field concentrating on the areas near the focus in the Fresnel region of an f/12 system using optical wavelengths. Computer predictions were made for four cases: unapodised-unaberrated, apodised-unaberrated, unapodised-aberrated, and apodised-aberrated. Predictions were made for cross-sectional planes perpendicular to the optical axis using Fourier optics. Meridional plane predictions were produced using a numerical integration method of determining the Kirchoff integral. Additionally, experimental data are given to compare with the predictions. It is shown that the experimental data matches the computer predictions and that apodisation is an effective method for controlling the ringing due to edge effects and spherical aberrations. Additionally, fine structure corresponding to Young's double slit interference is observed in unapodised cases.

END

12-86

DTIC